OPTICAL FEEDS FOR PHASED ARRAY ANTENNAS

by

Cathy Wood Leonard

Thesis submitted to the Faculty of the
Virginia Polytechnic Institute and State University
in partial fulfillment of the requirements for the degree of

Master of Science
in
Electrical Engineering

APPROVED:

R. O. Claus, Chairman

W. L. Stutzman

T. Pratt

December 1988

Blacksburg, Virginia

OPTICAL FEEDS FOR PHASED ARRAY ANTENNAS

by

Cathy Wood Leonard

Electrical Engineering

Abstract

This thesis investigates optical feed methods for phased array antennas. The technical and practical limitations are analyzed and an optimum design is determined. This optimum optical feed is a two-beam interferometric approach which uses acoustooptic phase control. The theory is derived; a computer model is developed; and the limitations are determined. Design modifications are suggested which reduce limitations and greatly extend the range of applications.

TABLE OF CONTENTS

CHAPTER 1. INTRODUCTION

To satisfy the requirements of scanning a narrow beamwidth, the large, turning radar dish was developed. However, the mechanical steering is a slow, expensive, power consuming process. In the 1960s, the phased array antenna was designed to combat these mechanical problems. The replacement of a single, movable antenna with an immobile array of radiating elements offers the advantages of rapid electronic beam steering and increased reliability. The radiation pattern is steered through space without moving the antenna itself. This is accomplished by changing the phase of the excitation currents in each element of the array. The relative phase of the excitations determines the resulting beam direction.

Present-day phased array antennas are controlled by microwave phase shifters that are fairly lossy, bulky, and expensive. In future versions of the antenna, it is hoped that the conventional shifters will be replaced by smaller lower-power devices (such as optical devices) and that most of the bulky microwave waveguides will be eliminated. The optical/microwave antenna is an intriguing new kind of phased array antenna that uses fiber-optic transmission lines in the antenna feed in lieu of microwave guides. This hybrid antenna offers the prospect of improved control by transferring control to the optical domain.

The purpose of this thesis is to investigate optical feeds for phased array antennas and determine the optimum design. Several optical feed configurations are presented in Chapter 2. This chapter gives an overview of current research efforts in optical/microwave antenna technology. The technical and practical limitations are determined for each proposed method. Chapter 3 presents the two-beam interference method which was found to be superior to other optical feeds. The theory is derived; system design considerations are determined; a computer model is developed; and limitations are analyzed. Chapter 4 presents the thesis conclusions.

CHAPTER 2. OPTICAL BEAMFORMING/STEERING METHODS

Conventional techniques for implementing large phased arrays have resulted in heavy, high loss distribution systems. Monolithic Microwave Integrated Circuits (MMICs) have offered the ability to have a light-weight, low loss distribution system; however, the signal distribution and processing still present a challenge. Conventional feeds, using waveguides and coaxial cable, are impractical, especially in space or airborne applications. They encounter numerous problems including: 1) difficult design of the N-way power splitter driving all elements from one source; 2) diode phase shifters and their control; 3) a hardware and weight concentration at the aperture backplane; 4) the limited space available for signal distribution; 5) electromagnetic interference (EMI); and 6) crosstalk.

In an effort to utilize the advantages of MMICs, optical techniques are being developed. These techniques employ optical components not only to distribute signals, but also to create the phase and amplitude distribution. Fiber optics offers immunity to interference, excellent crosstalk isolation, small size and weight, and large bandwidth. Just as in conventional RF feed networks, there are two general approaches to optically controlled phased array antennas: time-delay beamsteering and phase-shift beamsteering. The bandwidth requirement of the particular system determines

whether time delay or phase control is used.

2.1 Time-Delay Beamsteering

Time delayers require long transmission paths but are necessary for applications requiring wide instantaneous bandwidth. Electronic time-delay devices do not compare to optical time-delay methods in satisfying several requirements for phased-array antennas: compactness, simplicity, remote invulnerable transmission, multi-gigahertz bandwidth, constant amplitude, ultra short delays, and rapid delay updating. Introducing time delays in the optical domain can lead to simple beamsteering networks, thus reducing the need for complex beam control methods. Four optical domain time-delay methods are investigated in this section.

2.1.1 Fiber Stretching

The optical feed subsystem of Figure 2.1, developed by Herczfeld, et al., consists of a signal and a reference link [1]. The fiber optic signal link is for data transmission to a remotely located active module; the reference link provides the frequency and phase reference for sychronization of a 38.89 GHz IMPATT oscillator. In this reference link, a piezo-electric transducer (PZT) is used to achieve a true time delay phase shift. The fiber is wrapped several

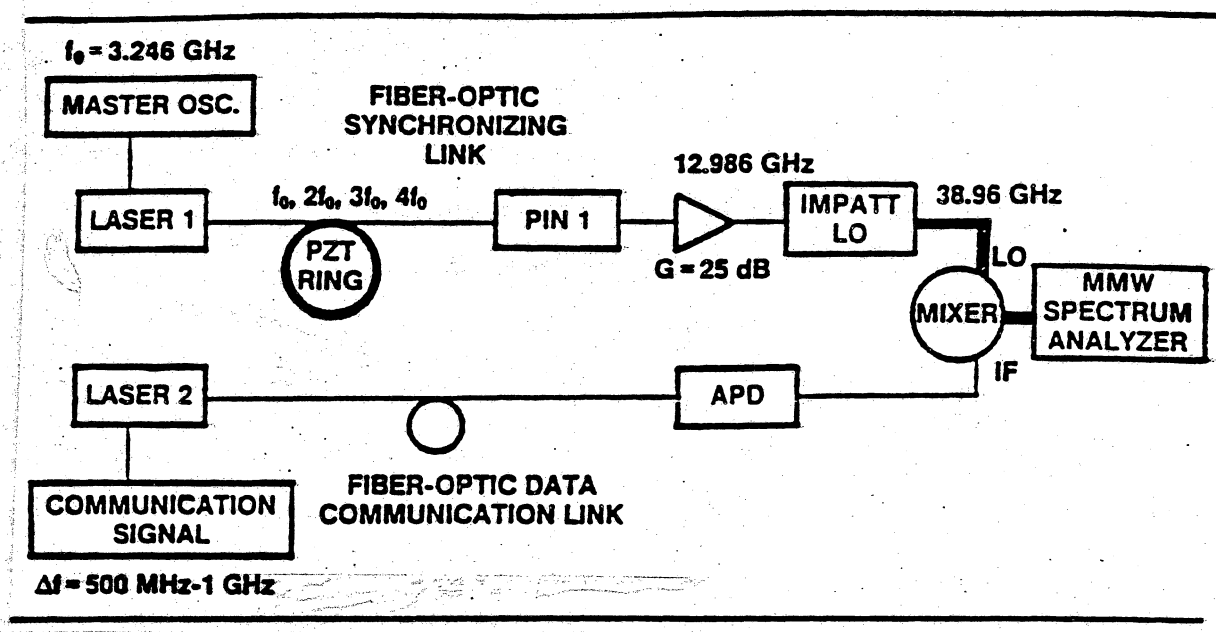

Figure 2.1 Optical feed using a PZT to stretch the fiber which produces the desired time delay [1].

times around the PZT. A high voltage DC supply provides the biasing voltage for expansion of the PZT ring, hence causing the fiber to stretch. This expansion introduces a variable time delay for the phase reference signal. A phase shift of 20 degrees at 10 GHz was obtained.

Although the feasibility of fiber optic links to achieve communications at the millimeter-wave frequencies is demonstrated by this system, there are problems which may render it somewhat impractical for phased arrays. First, only small phase shifts are possible. Also, due to the capacitance of the PZT crystal, the time constant necessary for the PZT and fiber assembly to relax back to the original phase was measured to be as long as two minutes. Another unknown factor concerns the reliability of continually stressing the fiber. Also, because the links were separate and not injection-locked, vast phase errors were observed. It is suggested that injection-locked, phase-locked loops should be considered.

2.1.2 Mode Coupling

Herczfeld, et al. also proposed the concept of a mode-dependent, programmable time-delay device [2], shown in Figure 2.2. In the step index multimode fiber, different modes travel with different velocities. Lower-order modes traveling along the fiber center take a shorter time to transit than the higher-order modes which are continually

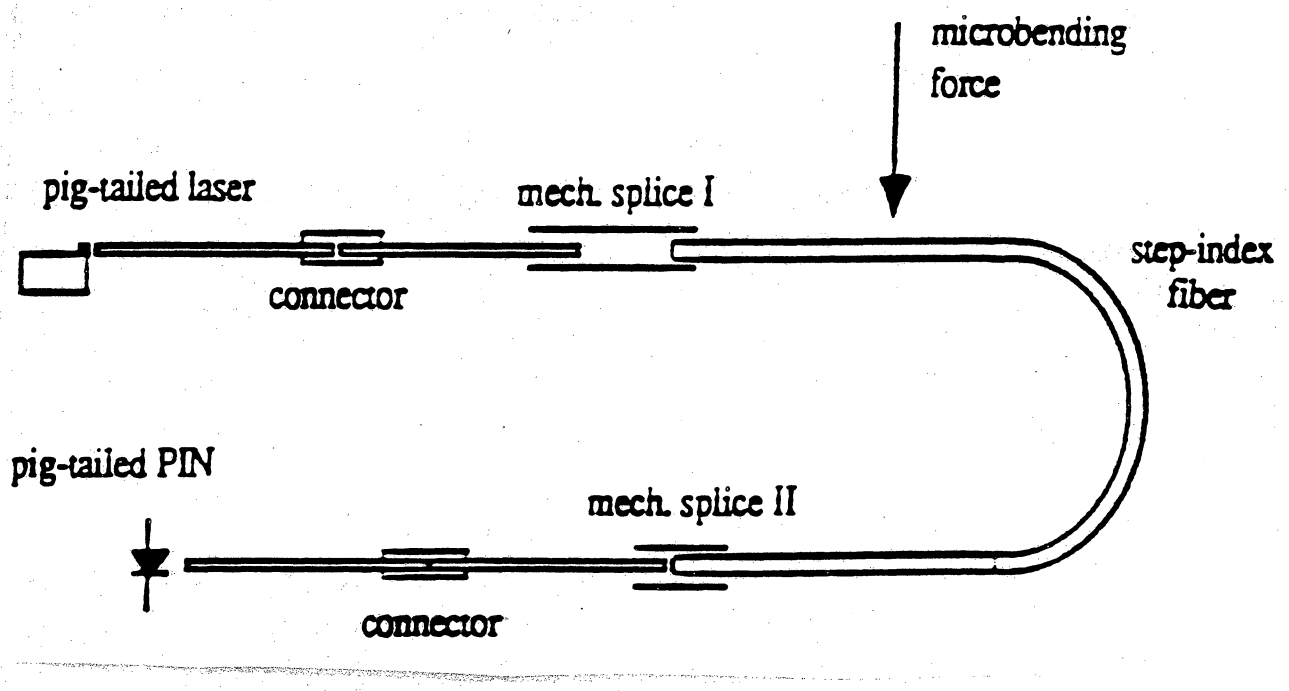

Figure 2.2 Induced mode coupling system to produce the desired time delay [2].

reflected at the core-cladding interface. Thus, the optical path is longer for the higher-order modes. By perturbing the fiber, a group of lower-order modes is redistributed to higher-order modes and a time delay is observed.

Multiple time delays may be accomplished by placing independent microbenders at selected locations on the fiber. The fiber could be coiled and the perturbers could be grouped on the coil form. When such a fiber is provided for each array element, linear time delays in the feed lines produce progressive phase shifts. When electromechanical deformers are employed, switching times are a few milliseconds. For electronic mechanisms, switching times in the microsecond range can be obtained.

Theoretically, it is possible to feed a phased array antenna by linking several mode-dependent time-delay devices of this type in parallel. However, the practicality of such a system is questionable. N array elements would require N lasers, all of which must be injection locked to reduce phase errors. Thus the number of elements that can be accomodated is severely limited.

2.1.3 Wavelength Varying

Figure 2.3 shows a wavelength dependent, tunable, optical time delay system developed by R. Soref [3]. By selectively varying the wavelength of the optical signal, the electrical signal is effectively and rapidly time delayed as desired.

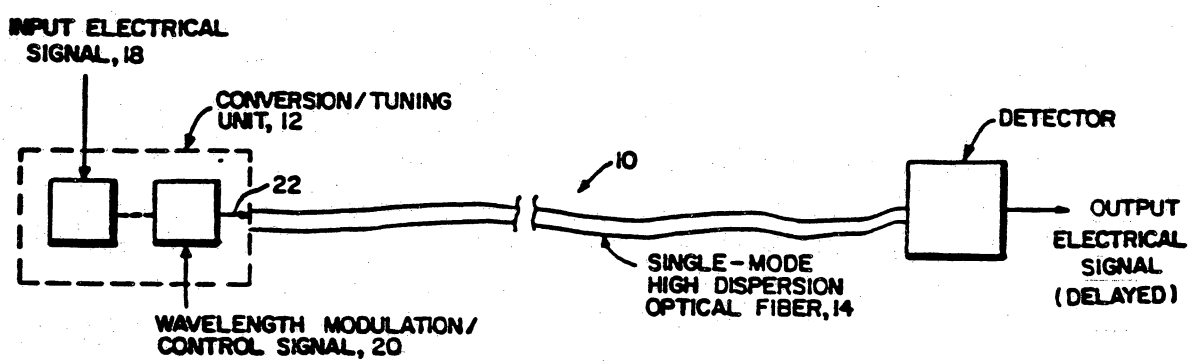

Figure 2.3 Wavelength dependent optical time delay system [3].

A cleaved coupled cavity laser operates in any one of several longitudinal modes and is capable of obtaining stable, single frequency oscillation in any one of the modes. The adjacent modes are separated by a few nanometers and cross talk is extremely low. This laser is directly modulated by a microwave input signal which is to be time delayed. By the further application of a wavelength modulation signal, the output is in the form of an optical signal at various wavelengths. The wavelength can be switched as rapidly as 7 nanoseconds by supplying current steps of a few milliamps.

The modulated laser output is fed into a single-mode, high dispersion optical fiber which exhibits a large chromatic dispersion over the wavelength band of interest. Consequently, as the wavelength is modulated or tuned, the speed at which the optical signal traverses the fiber is varied. The speed and thus the time delay is proportional to the wavelength. The fiber output is received by an optical detector which converts the optical signal back into an electrical signal. This reconstituted signal has the same waveform as the original microwave signal, only it is delayed. The delay can be adjusted even further by tailoring the length of the fiber.

It is possible to link several of such time delay systems in parallel for the purpose of feeding a phased array antenna. By providing progressive input wavelength modulation signals, progressive time delays of a single input electrical signal can be obtained. Thus, the resulting

antenna beam is steered to a proportional angle. Or, providing identical wavelength modulation signals would produce identical, in-phase outputs; in which case, the resulting antenna beam would be broadside. While theoretically feasible, such a system encounters the familiar practical and technical problems of injection locking N expensive lasers to feed N antenna elements.

2.1.4 Fibers Length Varying

With the growing interest in antennas that can produce multiple beams, a beamfomer based on the use of optical fibers as signal delay devices has been developed by Forrest, et al. [4]. The delay line structure is presented in Figure 2.4. To achieve the required pointing direction of each beam, a fiber delay line is used between each beam port and each element port. The required phase at each element port is produced by controlling the relative lengths of the fibers. A broadside beam, for example, is formed when the lengths are equal. Multiple simultaneous beams are formed by the addition of several parallel fibers at each beam port. At each detector, a summation of these beams occurs and the desired superposition of electrical currents is produced.

The number of optical souces required equals the number of simultaneous beams desired. The sources may be light emitting diodes (LEDs) or lasers; although lasers are preferred because of their higher output power and higher frequency operation. When lasers are employed, the operating frequency

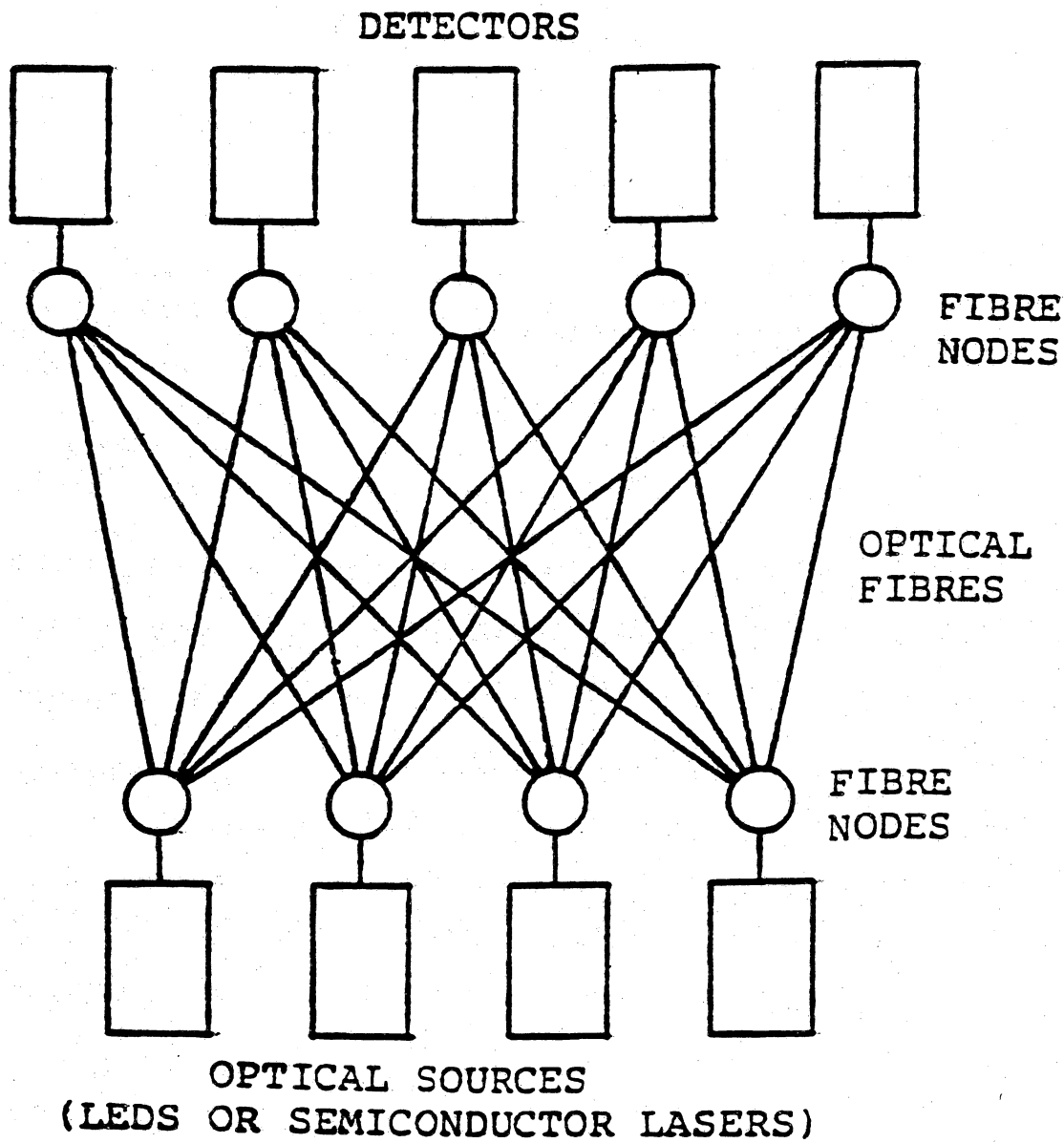

Figure 2.4 Fiber delay line structure for feeding a phased array antenna [4].

can be directly at RF up to several gigahertz. The beamformer can be operated at an intermediate frequency; however, the usuable bandwidth is severely limited and the system requires upconverters at each element.

The phase accuracy is characterized directly by the accuracy to which fiber lengths can be cut. The amplitude accuracy is the critical parameter, being dependent upon the N-way power split accuracy (uniformity) of the star couplers used at the fiber nodes. With today's coupler fabrication techniques, uniformities on the order of 10 to 15 percent are available for six port couplers [5].

Although this system appears feasible for antenna arrays, the number of elements that can be accomodated is severely limited by the coupler capability. Multimode 32 X 32 star couplers are commercially available, but the attainable uniformity is not adequate for the array requirements. For large arrays, beam expanders could be used in place of the couplers at the fiber input nodes. This would provide an area of uniform illimination as large as the area of a fiber bundle. It is suggested in [4] that a large area (60 mm^2) photodetector at the fiber bundle output would be sufficient to achieve a good uniformity of light collection. However, due to the increased capacitance and the resulting increased noise, the system signal-to-noise ratio degrades. Thus, without improvement in fiber node techniques, this type of feed system may not be viable, even for relatively small arrays.

2.2 Phase-Shift Beamsteering

Since phase is the product of frequency and time delay, phase-shifters are highly frequency dependent. The critical difference between phase and time delay, as used in arrays, is the fact that phase is computed on the basis of modulo 2π; that is only the fractional part of the total number of cycles of phase is used. For antennas with an instantaneous microwave bandwidth of 2 percent or less, phase shift steering will give accurate beampointing [6].

2.2.1 Optical Injection of Semiconductors

The common ground to microwave and electrooptic devices is the PIN diode. Microwave devices and monolithic circuits are fabricated from high resistivity materials which are also sensitive to optical excitation. Rosen et al. have developed an optically controlled beamforming method for phased array antennas using a modified microwave PIN diode equipped with an optical port [7 - 9]. This port acts as a third terminal through which the device parameters can be controlled. Light is injected into the intrinsic region generating electron-hole pairs which change the conductance and capacitance of the device. The amount of phase shift attainable is directly related to the range of capacitance

change that can be achieved. Two such structures were investigated.

The first optically controlled microwave PIN diode phase shifter was of the mesa type shown in Figure 2.5 [7]. This structure achieved 20 degrees of phase shift over a 15 percent bandwidth centered at 10 GHz. The device exhibited high resistance, however, and was relatively insensitive to illumination because of limited exposure of the intrinsic region.

A lateral PIN diode, Figure 2.6, led to much improved characteristics [8]. This PIN geometry lends itself to efficient exposure of the entire intrinsic region to optical excitation and is compatible with conventional integrated circuit technology. The devices demonstrated capacitances as low as 0.1 picofarad and forward-biased RF resistances as low as 1 ohm. The optical control is provided by a semiconductor laser coupled through an optical fiber positioned and adjusted above the intrinsic region of the lateral diode. Phase shifts of between 110 to 120 degrees over the range from 4 to 8 GHz were obtained experimentally. However, for higher frequency operation, a lower capacitance diode and more complex circuitry is required.

A similar, but improved, device was proposed in 1987 by Brothers et al. [10]. This design is based on optical injection of an optical PIN rather than a microwave PIN, thus no modification is required to increase optical sensitivity. Figure 2.7 shows the configuration of the phase shifter. The photodetector junction area is small, resulting in a more

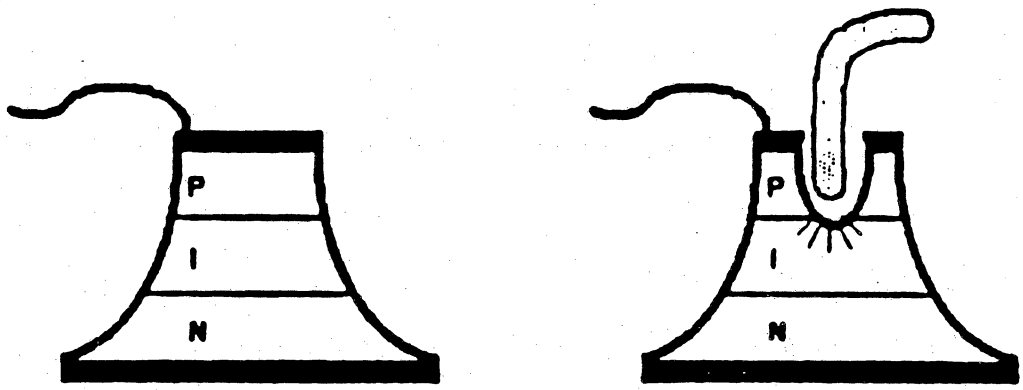

Figure 2.5 Microwave PIN modified to a mesa structure for optical control of the phase shift [7].

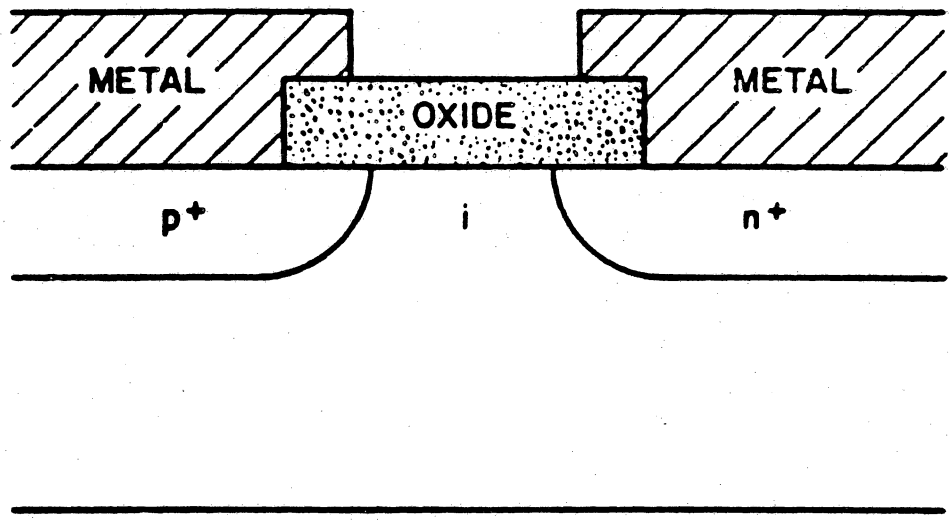

Figure 2.6 Lateral PIN modified for optical phase control [8].

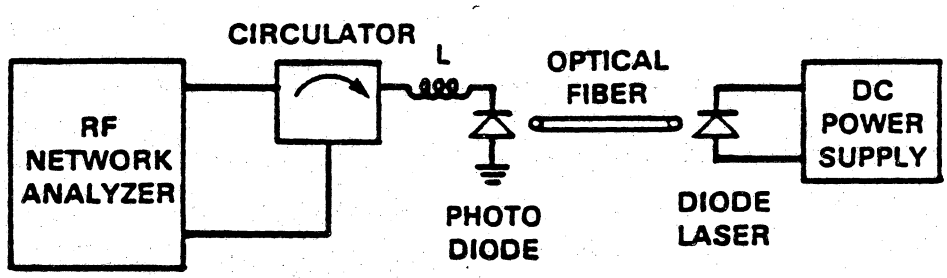

Figure 2.7 Unmodified optical PIN phase shifter [10].

efficient illumination area. A semiconductor laser is used as the optical source. With zero bias applied to the PIN, capacitance changes of 30 picofarads were obtained corresponding to 180 degrees of phase shift at an RF operating frequency of 260 MHz. By applying 0.1 volt of forward bias, a phase shift of 245 degrees was measured. An important experimental result is that the capacitance is linearly related to the optical power in this design. As with previous proposals, however, the RF operating frequency is limited by the device capacitance. Operation at frequencies above a few GHz would require fabrication of PINs with a smaller minimum capacitance and a wider bandwidth under high-level injection. Brothers suggests that scaling the device geometry to produce a minimum capacitance of 0.1 picofarad would allow for a 180 degree phase shifter at frequencies up to 14 GHz.

2.2.2 Interferometer With Electrooptical Phase Shifter

A voltage controlled optical/RF phase shifter proposed by Soref [11] is shown in Figure 2.8. In this interferometric approach, an optical frequency translator in one leg upshifts or downshifts the intial laser frequency. An electrooptical phase modulator (EOM) is inserted in one leg to control the relative phase. When the two beams interfere and are incident on the detector, a beat frequency is produced with its phase set by the EOM. The detector's electrical output

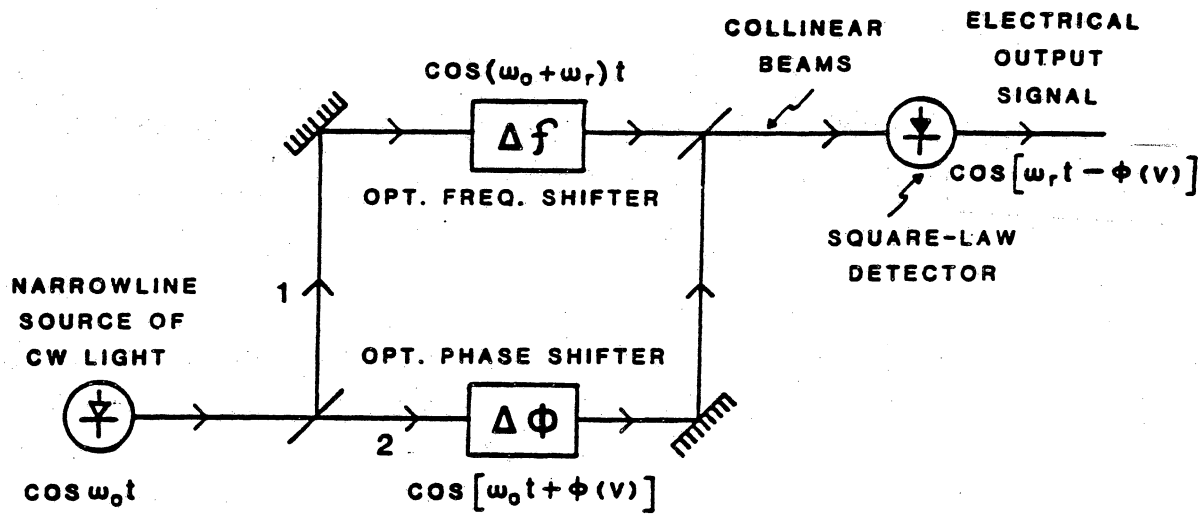

Figure 2.8 Optical interferometer with a voltage controlled electrooptical phase shifter [11].

signal is produced by coherent mixing of two light beams. As the voltage applied to the EOM is varied, the electrical phase shift varies proportionally. Operation was verified at 125 MHz. By stepping the EOM voltage from -1200 V dc to +1200 V dc, the RF phase shift was varied from -2π to 2π.

While the technical feasibility of such a phase shifter has been demonstrated, it is suggested that its practicality would require integrated-optics technology to produce a compact, low-voltage circuit. Another constraint is the operating frequency. This is limited to the frequency of the optical frequency translator, which is less than 4 GHz, maximum. Also, N of these configurations would be required to feed an N-element phased array. For large arrays, the cost of the lasers alone would appear to eliminate the system from consideration.

2.2.3 Two Beam Interference With Fiber Array

Another interferometric approach makes efficient use of the optical interference pattern by using a fiber pick-up array. The design was first proposed and conceptually tested by Koepf [12]. The phase is controlled acoustooptically. Only a handful of components is required to feed a large antenna array. Due to its simplicity, uniqueness, and efficiency, this optical feed approach was found to be superior to any of the other proposed methods. The design is presented and analyzed in Chapter 3.

CHAPTER 3. THE TWO-BEAM INTERFERENCE METHOD

3.1 System Basis

A fiber optic feed proposed by Stillwell et al. [13] at Naval Research Laboratory (NRL) uses Koepf's ideas [12] as its basis. It involves two, plane, optical wavefronts impinging on the fiber optic pickup array. This beam generating subsystem, which will be called OFEED, is shown in Figure 3.1. A coherent light source, when properly modulated and combined with a reference beam, will produce a microwave amplitude modulated optical pattern at the optical transform plane. This two-dimensional Fourier transform is performed in real time by far-field diffraction of the coherent light. Optical wavelengths are approximately 1E-6 smaller than RF wavelengths, so far-field diffraction can be generated in a space a few millimeters long rather than many meters. This optical pattern is the analog of the needed microwave excitation pattern.

In Figure 3.1 the two optical beams generated by OFEED differ both in frequency and in direction of propagation. The difference frequency is obtained by injection locking a slave laser with the emission of a master laser; the master laser is frequency shifted by a Bragg cell operating at the desired transmit frequency. Thus, the frequency difference

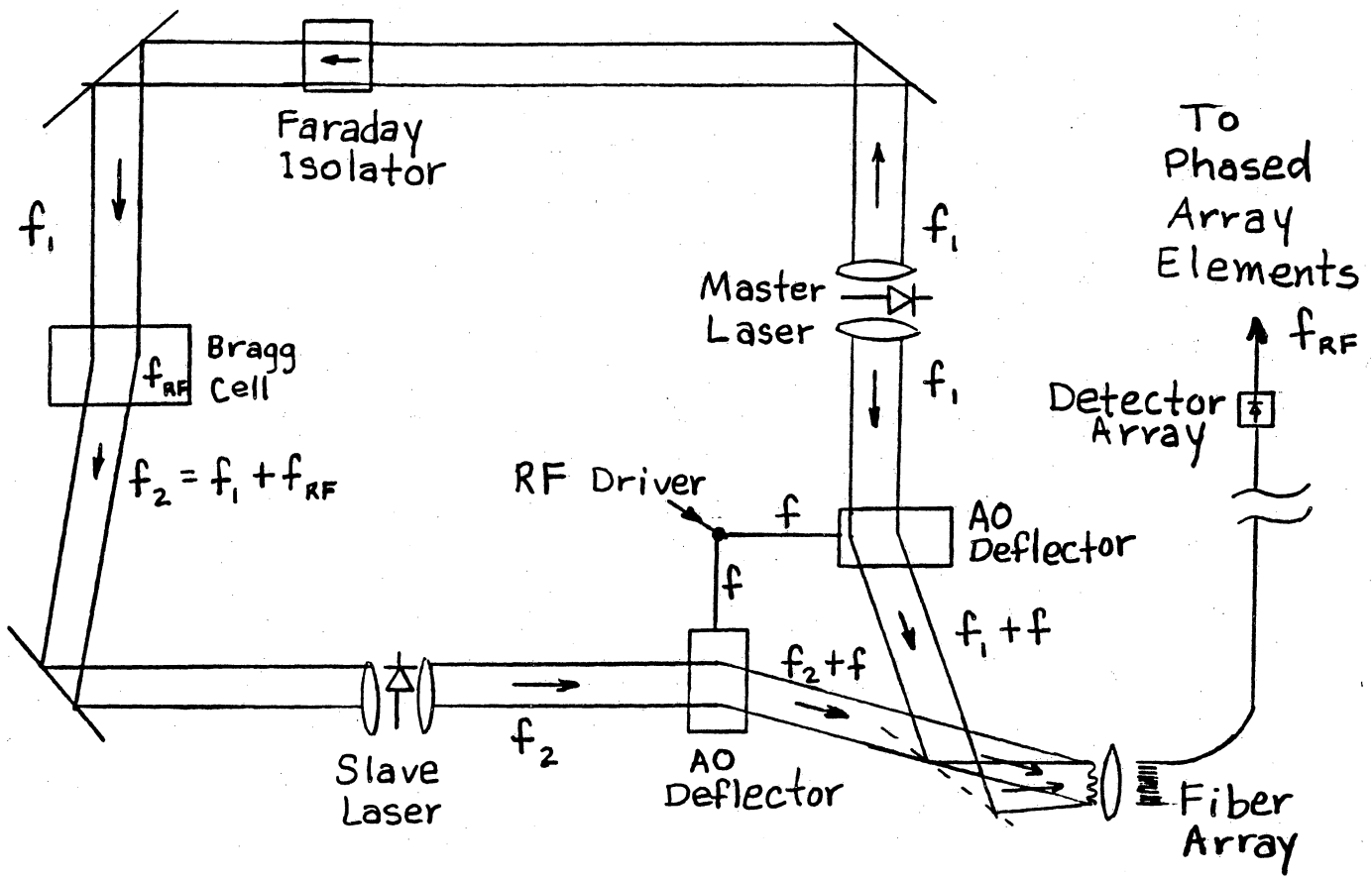

Figure 3.1 Two-beam optical interference feed [13].

in the two beams is the operating frequency of the Bragg cell. The antenna beam is steered by controlling the interference angle of the two optical beams. This is accomplished by sweeping the drive frequency of two acoustooptic (AO) modulators, one in each leg of the beam simulator.

The optical pattern generated by beam interference is incident on the fiber array, as shown in Figure 3.2. Due to the interference phenomenon, the difference in phase between the two beams is converted to an intensity variation. At any instant, a linear phase progression exists across the fiber inputs. Each fiber is in one-to-one correspondence with a similarly positioned antenna element. An optical-to-microwave conversion must take place before the antenna array can be driven. This is accomplished by photodetectors, one at each fiber output. Since photodetectors are square-law devices, the phase of a light field can only be detected by the addition of a second light field, which acts as a phase reference. Thus, the generation of two interfering beams in OFEED results in an intensity variation which is translated to phase detection by the photodetectors.

Each detector generates a current oscillating at an RF frequency equal to the difference frequency $(f_2 - f_1)$ with an amplitude and phase determined by its position in the array. These currents drive the full sized phased array antenna. The antenna array then produces a radiation pattern which is the Fourier transform of its excitation. Thus, the system accomplishes two transforms: the first, an optical

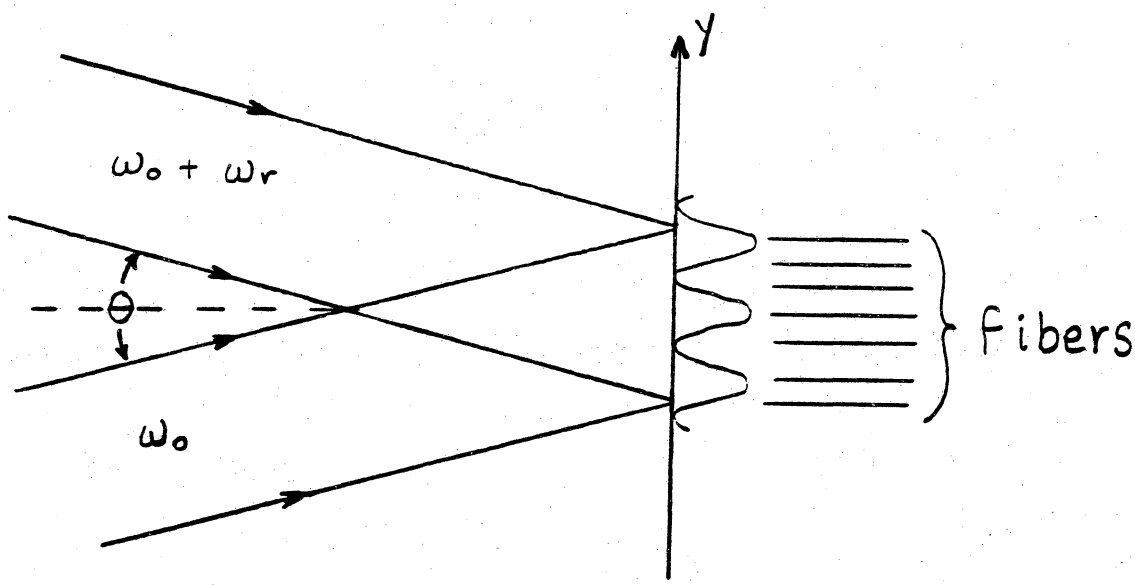

ω_o = optical angular frequency

ω_{rf} = angular RF

Figure 3.2 Far-field optical interference pattern.

one produced by the beam generating subsystem; the second is performed by the antenna itself. By sweeping the drive frequency of the AO deflectors, the beam interference angle is scanned and the final microwave main beam position moves over some solid angle in the far field with a one-to-one correspondence between points.

By using a natural property of coherent light, this optical feed design is unique and much simpler than others proposed. The requirements for Monolithic Microwave Integrated Circuits (MMICs) used with this feed system are greatly reduced. No separate variable phase shifters (VPSs) or variable power amplifiers (VPAs) are necessary. There is no need for control lines. In fact, the only function required is signal amplification; and, even this is reduced or eliminated when avalanche photodiode detectors (APDs) are employed in the feed system.

Mathematically, the operation of the feed system is quite analogous to the operation of the antenna array itself, its basis being that the far-field pattern is the Fourier Transform (FT) of the near-field distribution.

3.2 Theory of Operation

The operation of the optical feed subsystem can be understood by considering the wave nature of light. The phenomena of coherence, interference, and diffraction form

the basis of this type of feed system.

3.2.1 Coherence

Interference patterns of light from two sources can be observed only if the sources are coherent. By definition, coherent sources are in phase or have a phase difference that is constant in time.

In comparison, in incoherent sources, the phase fluctuates randomly. Many fluctuations occur during a time interval making it impossible for any detection device to respond to the rapid intensity changes. Thus, only the average value is seen and there is no possibility of observing an interference pattern.

For two coherent sources of equal strength, the intensity at any instant is proportional to

$$4 A_o^2 \cos^2 \tfrac{1}{2} \delta \qquad (3-1)$$

where A_o is the amplitude of each wave separately. The phase difference, δ, is a function of time. If δ varies rapidly, as in incoherent sources, only the time average of

$$4 A_o^2 (\cos^2 \tfrac{1}{2} \delta)_{av} = 2 A_o^2 \qquad (3-2)$$

will be observed [14]. There is then no observable interference pattern when the sources are incoherent.

The sources in OFEED are injection locked lasers. The constant phase relationship between the two lasers in Figure 3.1 is set by the Bragg cell. Its frequency determines the oscillating frequency of the resulting interference pattern.

The beam steering function is realized by the diffraction phenomenon occurring in the AO modulators.

3.2.2 Diffraction

If a wave is partially blocked by an opaque barrier or an aperture, the apparent direction of travel will be altered. This bending of the path is called diffraction. Diffraction is actually a kind of interference. Waves from one part of the opening interfere with waves from another part to produce the diffraction pattern. The maxima and minima which appear in the pattern indicate that interference is taking place. It is the finite size of an aperture which is responsible for diffraction effects; thus, an unrestricted wave does not produce a diffraction pattern. In OFEED this diffraction occurs in the AO modulators.

Thus the AO modulator serves as a phase grating. The resulting far-field diffraction pattern is determined by the number of lines in the grating, their spacing, and their width. Because of its importance in OFEED, a standard treatise of far-field diffraction theory [15] is presented in Appendix A.

When AO modulators are employed to effect the diffraction

process, as in OFEED, acoustic parameters must also be taken into account.

3.2.3 Acousto-Optic Diffraction and the Bragg Regime

The diffraction of light by acoustic waves in liquids and solids has been extensively studied both experimentally and theoretically [16]. Several factors have generated intensive interest in the subject: the invention of lasers as coherent light sources, the development of high-frequency acoustic transducers, and the development of materials having excellent acoustic and optical properties and large photoelastic constants. Acousto-optic devices have been developed for the purpose of optical beam control, such as the Bragg cell and the AO deflectors in the subject system OFEED.

The acoustooptic materials are transparent over the optical wavelength range of interest (0.7 - 1.6 micrometers) and have negligible insertion loss. Periodic density changes are produced in the AO modulators by an acoustic wave. This causes periodic refractive index changes due to the photoelastic effect.

There are two important regimes for acousto-optic interactions: the Raman-Nath scattering and the Bragg diffraction regime. Raman-Nath diffraction occurs at relatively low frequencies when the acoustic beam width along the optical propagation direction is small. As illustrated

in Figure 3.3, when this beam width (grating length i) is sufficiently small, the incident beam will be partially diffracted from the zero-order into a multiplicity of higher orders [17].

If, however, the interaction length, i, is sufficiently large, the process enters the Bragg regime. Here, the zero-order beam will be partially deflected into only one order, as shown in Figure 3.3(b). This degree of control is required in the subject system in order to steer the beam efficiently and accurately. The key parameter is

$$Q = \frac{2\pi L\ i}{n\ \Lambda} \qquad (3\text{-}3)$$

where

i = interaction length of acoustic wave column

n = index of medium

Λ = acoustic wavelength

L = optical wavelength

When $Q < 1$, the Raman-Nath regime dominates; when $Q > 7$, Bragg diffraction occurs and the output light wave can then be approximated by the first-order term. A plot of the relative output intensity would be similar to the diffraction pattern of Figure A.2. However, due to the presence of some acoustic wave attenuation, the pattern will have a slightly larger half-power beamwidth and somewhat larger sidelobe level.

In an acousto-optic deflector operating in the Bragg

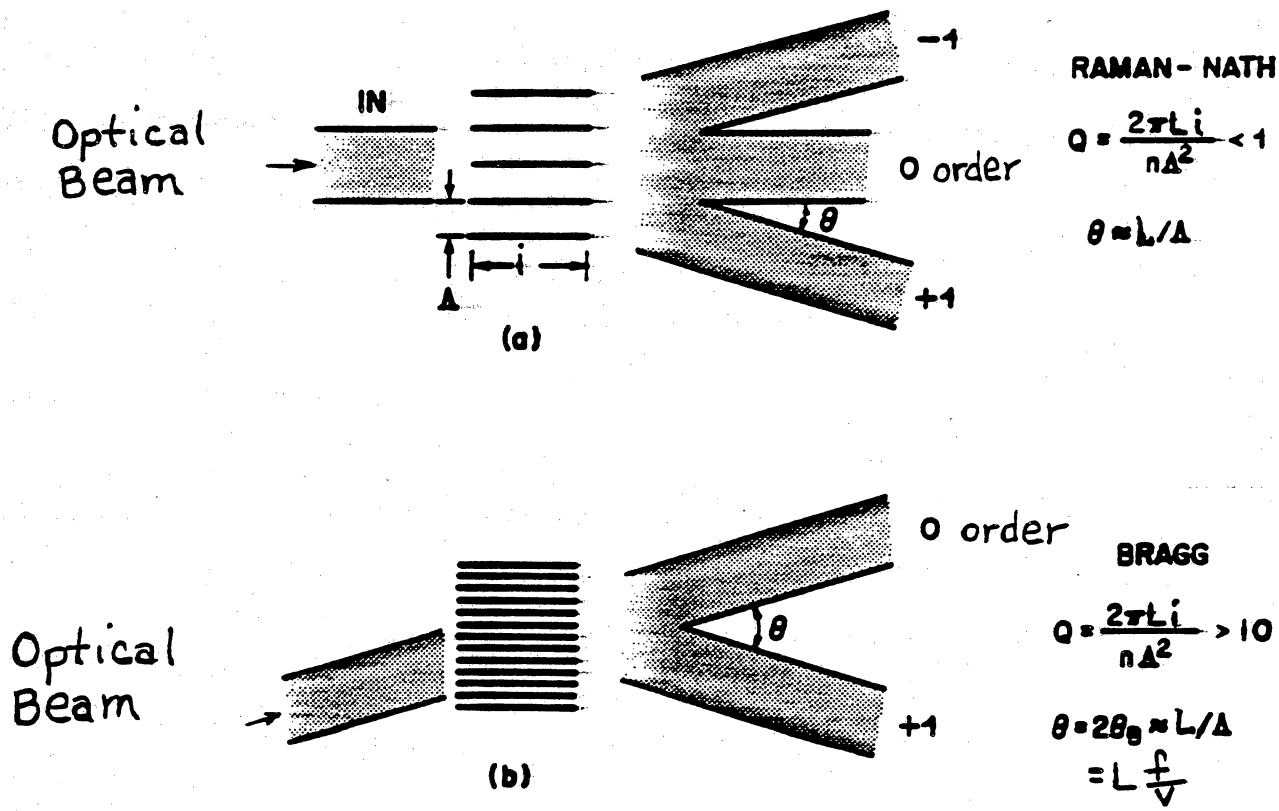

Figure 3.3 Acousto-optic diffraction regimes [17].

regime, the incident optical beam is diffracted into only one order. The resulting output light rays are approximately parallel in the far-field. As shown in Figure 3.4, the path difference for the rays from adjacent lines is d sin θ, where d is the line separation and θ is the output angle of the first order beam with respect to the zero order beam. If this path difference is an integral number of wavelengths, the rays from all layers will be in phase and a strong wave will occur at angles which satisfy:

$$d \sin \theta = m L \qquad (3\text{-}4)$$

where m is the diffracted order. This equation is identical to equation (A-13) which locates where the maxima occur in a diffraction pattern. Since the beam is deflected into only one order, however, the m in the above equation can be omitted.

Now, in an AO deflector, the line separation can be represented in terms of the acoustic wavelength, i.e. d in Figure 3.4 equals Λ. Substituting into (3-4) gives:

$$\sin \theta = L/\Lambda \qquad (3\text{-}5)$$

or for small angles:

$$\theta \approx L/\Lambda \qquad (3\text{-}6)$$

Alternatively, this can be represented in terms of the

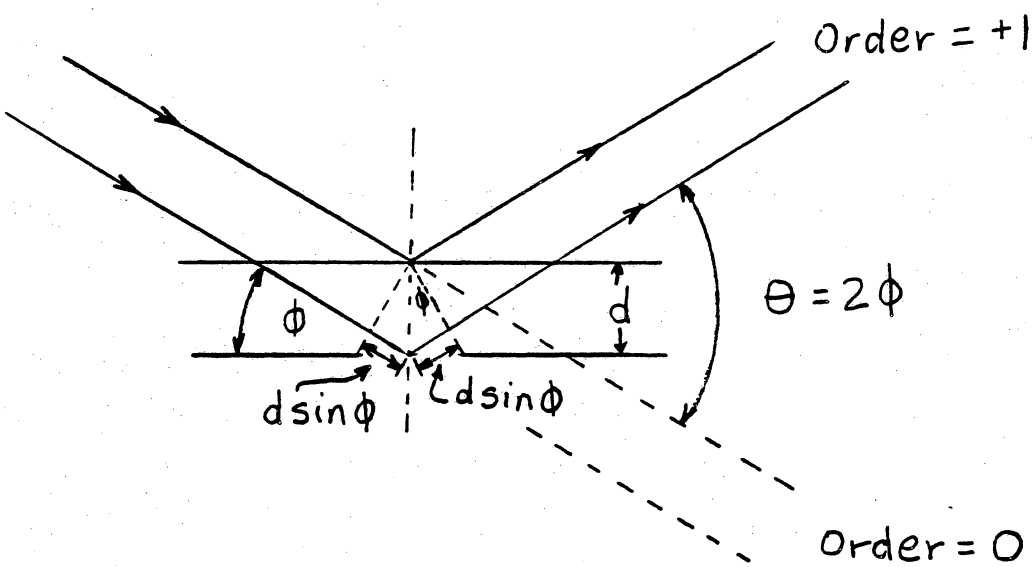

$$\text{path difference} = 2d\sin\phi$$
$$= 2d\sin\frac{\theta}{2}$$
$$\simeq d\sin\theta \quad \text{for small } \theta$$

Figure 3.4 Path difference for rays from adjacent slits.

acoustic frequency, f, and the acoustic velocity, v:

$$\Theta \approx L\, f/v \qquad (3\text{-}7)$$

Thus, the important result is that the diffraction angle is proportional to the acoustic drive frequency (f); and the optical beam can in fact be steered by sweeping this frequency. This in turn, steers the antenna beam. The angle of the antenna beam is proportional to the small angle at the output of the AO deflector; but, it is considerably magnified by the antenna geometry, as will be discussed in section 3.2.6.

2.2.4 Interference

In OFEED, phase detection by the photodetectors is possible when the input to the detectors is a two-beam interference pattern. The interference angle of the two beams is controlled by diffraction in the AO deflectors. The beams are generated by two coherent sources (lasers) which maintain a difference frequency by injection locking techniques. The interference pattern can be analyzed then by considering the superposition of two waves of nearly equal frequency and wavelength.

According to the principle of superposition, if light waves from two different sources are radiating through a common medium, their amplitudes will add if the medium is

linear. This concept is illustrated in Figure 3.5. The beams from the two lasers in this system can be represented by [15]:

$$E_1 = A_o\, e^{j(w_o t)} \qquad (3\text{-}8)$$

$$E_2 = A_o\, e^{j((w_o + w_r)t - \delta)} \qquad (3\text{-}9)$$

where

A_o = maximum amplitude

w_o = optical angular frequency

w_r = angular RF

δ = phase difference between beams

Then the resultant wave is found by adding the two fields.

$$\begin{aligned} E_T &= E_1 + E_2 \\ &= A_o\,[e^{j(w_o t)} + e^{j(w_o t + w_r t - \delta)}] \\ &= A_o\,(1 + e^{j(w_r t - \delta)})\, e^{j(w_o t)} \end{aligned} \qquad (3\text{-}10)$$

Figure 3.5 indicates that the envelope of the amplitude of the two-beam interference pattern varies sinusoidally at the difference frequency. The amplitude is a function of the relative phase between the two beams, δ, and is proportional to cos $\frac{1}{2}\delta$. The nodes in this figure correspond to a phase difference of 180° between the two beams. These nodes occur at half-wavelength spacings. The antinodes correspond to a 0° phase difference.

For a time-varying field, it is the average value rather

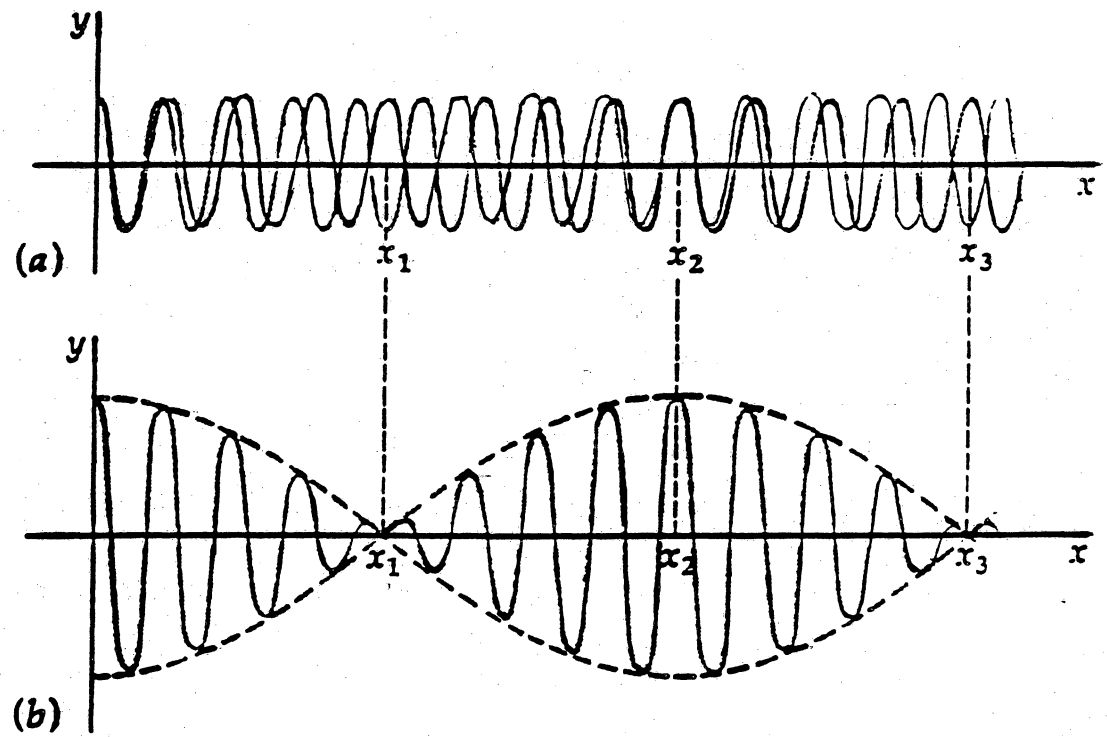

Figure 3.5 (a) Two waves with slightly different frequencies.
(b) Superposition of the two waves in (a) [14].

than the instantaneous energy which is the significant physical quantity. The average of the exponential term $e^{j(\omega_o t)}$ will vanish over one period since the positive and negative areas of this function are equal in magnitude. Thus, the intensity, I, of this time-varying field is defined by the relation [15]:

$$\begin{aligned} I &= \tfrac{1}{2}\, \mathrm{Re}\,(E_T\, E_T^*) \\ &= \tfrac{1}{2}\, A_o^2\, (1 + e^{j(\omega_r t - \varepsilon)} + e^{-j(\omega_r t - \varepsilon)} + 1) \\ &= \tfrac{1}{2}\, A_o^2\, (2 + 2\cos(\omega_r t - \varepsilon)) \\ &= A_o^2\, (1 + \cos(\omega_r t - \varepsilon)) \end{aligned} \qquad (3\text{-}11)$$

where Re is the real part. Note that the final expression can be written as a $\cos^2$ function using a trigonometric identity, in which case:

$$I = 2\, A_o^2\, \cos^2((\omega_r t - \varepsilon)/2) \qquad (3\text{-}12)$$

However, considering only the time-varying term of (3-11) and neglecting the dc component, as in an ac-coupled detector, the interference pattern can be expressed as:

$$I = I_o \cos\,(\omega_r t - \varepsilon) \qquad (3\text{-}13)$$

where the constants have been absorbed into I_o. Thus, the intensity varies sinusoidally at the difference frequency between the two sources, ω_r. The relative phase, ε, is a function of the interference angle between the

two beams.

3.2.5 Phase Correlation

In OFEED the intensity modulated signal represented by equation (3-13) is fed to the fiber array. The phase, ξ, is presented in Figure 3.6 and is defined by the relation [15]:

$$\xi = n\,\alpha \qquad (3\text{-}14)$$

where

n = $-M$ to $+M$ = array position number

α = differential phase separation $= 2\pi\Delta/L$

where Δ is the optical path difference between fibers and L is the optical wavelength. This path difference, Δ, can be determined from the geometry in Figure 3.6 as:

$$\Delta = 2\,b\,\sin\theta_H \qquad (3\text{-}15)$$

where

b = fiber spacing

θ_H = half angle between beams

This results in the differential phase between elements:

$$\alpha = 4\pi\,b\,\sin\theta_H / L \qquad (3\text{-}16)$$

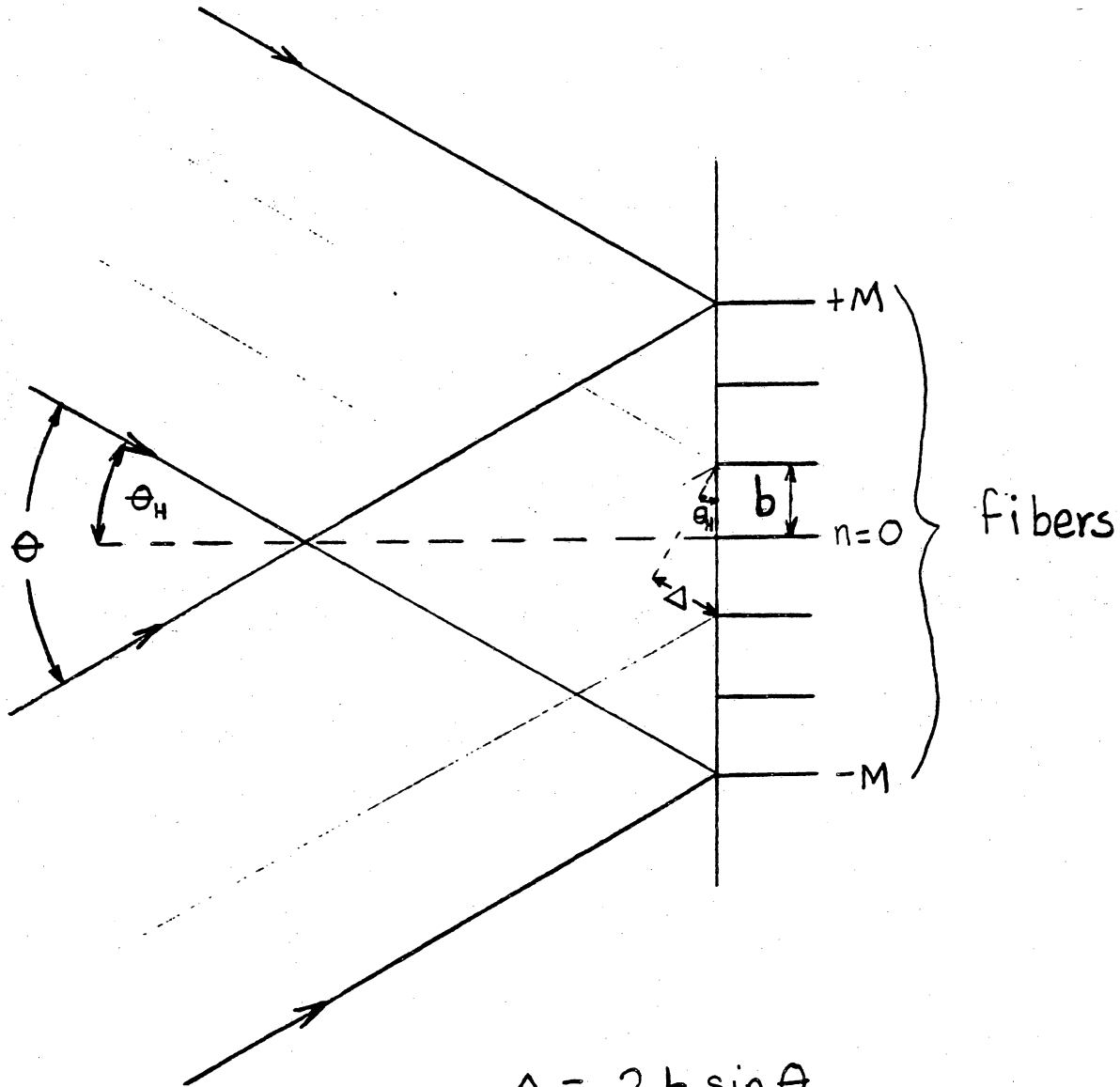

Figure 3.6 Phase, δ, as a function of the optical path difference between fibers, Δ.

The interference angle in this system is a very small angle such that $\sin\theta = \theta$. Then equation (3-16) can be written:

$$\alpha = 2\pi\, b\, \theta / L \qquad (3\text{-}17)$$

where now θ is the interference angle rather than the half angle.

This defines the phase difference between antenna elements. The antenna array geometry magnifies the interference angle θ and steers the beam to an angle θ_A which is proportional to θ. The differential phase in an antenna array as shown in Figure 3.7 is defined by [18]:

$$\alpha = 2\pi\, d \sin\theta_A / \lambda \qquad (3\text{-}18)$$

where

d = antenna element spacing

θ_A = antenna angle with respect to normal

λ = microwave wavelength

Here, θ_A is a larger angle and is not approximately equal to $\sin\theta_A$. Equations (3-17) and(3-18) are equal expressions of the phase: one in terms of the optical interference angle and the other in terms of the antenna steering angle. The magnification of the interference angle θ is found by setting (3-17) equal to (3-18). Then

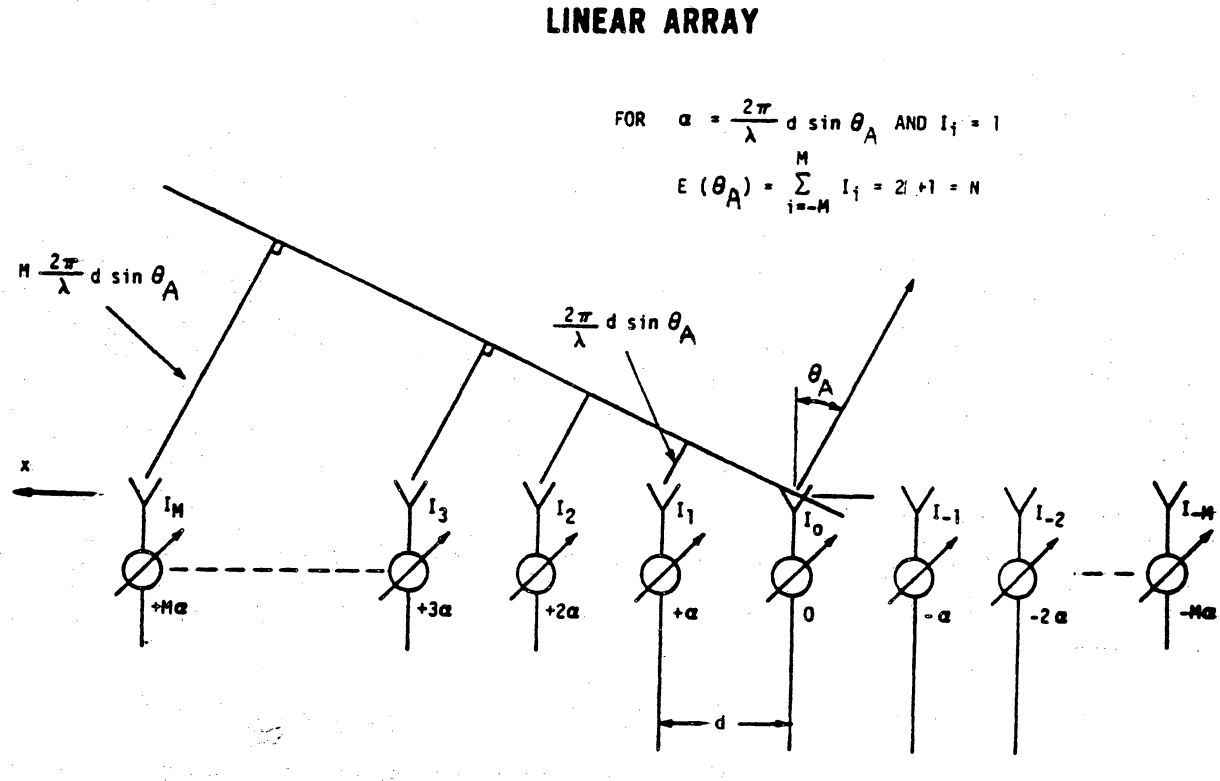

Figure 3.7 Differential phase relationship in an antenna array [18].

$$\frac{\sin\theta_a}{\theta} = \frac{\lambda}{L}\,\frac{b}{d} \qquad (3\text{-}19)$$

Now the optical interference angle, θ, is controlled by the AO deflectors. Recall from equation (3-7) that the deflection angle for an AO deflector is: L f / v where f is the acoustic drive frequency and v is the acoustic velocity. If the two AO deflectors in OFEED are driven with the same frequency, f, then the interference angle is just twice the deflection angle, or:

$$\theta = 2\,L\,f\,/\,v \qquad (3\text{-}20)$$

A modification of this expression will be used in the following section to simplify (3-19).

3.2.6 Phased Array Considerations

In phased array antenna systems, it is the scan angle that is the primary consideration. In OFEED, scanning the optical interference angle results in a proportional antenna scan angle. The optical scan angle is given by [16]:

$$\Delta\theta = 2\,L\,\Delta f\,/\,v \qquad (3\text{-}21)$$

where

Δf = scanned bandwidth of AO deflector

Then referring to (3-19), the antenna scan angle can be expressed as:

$$| \sin \theta_A | = \Delta\theta \frac{\lambda b}{L d} \qquad (3\text{-}22)$$

Making the substitution from equation (3-21) yields:

$$| \sin \theta_A | = \frac{2 \Delta f \lambda b}{v d} \qquad (3\text{-}23)$$

The absolute value of $\sin \theta_A$ implies that the antenna scan angle is $\pm\theta_A$. The sign of the angle is determined by the sign of Δf, which is positive if scanning the AO frequency from the low to the high value, and negative if scanning from the high to the low frequency.

In the resulting antenna radiation pattern, in-phase addition occurs at the angle θ_A. However, there can be more than one angle for which in-phase addition occurs. The other angles are called grating lobes and are generally undesirable. Grating lobes reduce the efficiency of the transmitting antenna and cause interference in the receiving antenna.

Grating lobes can be omitted by the correct choice of the ratio d/λ. This can be determined by examining the antenna array factor. Consider the antenna array factor for a linear phased array. At an angle θ with respect to normal, the value of this factor is [18]:

$$E(\theta) = \frac{\sin [\, N\, (\pi d/\lambda)\, (\sin\theta - \sin\theta_A)\,]}{\sin [\, (\pi d/\lambda)\, (\sin\theta - \sin\theta_A)\,]} \qquad (3\text{-}24)$$

where N is the number of elements in the array. The visible region of the pattern is defined as: $-1 \leq \sin\theta \leq 1$, which corresponds to $-90° \leq \theta \leq 90°$. Considering only the visible region then, grating lobes occur whenever the denominator in (3-24) equals zero (except when $\theta = \theta_A$, the main lobe). Equivalently, this occurs when:

$$(\pi d/\lambda)\, (\sin\theta - \sin\theta_A) = \pm i\pi \qquad (3\text{-}25)$$

where i is an integer. Thus, by properly choosing the ratio d/λ, grating lobes are suppressed. From this equation, the criterion for no grating lobes becomes [18]:

$$\frac{d}{\lambda} < \frac{1}{1 + |\sin\theta_A|} \qquad (3\text{-}26)$$

The ratio $d/\lambda = 0.5$ is usually quite sufficient for suppression of grating lobes. With this spacing, there is exactly one period of the array factor in the visible region. This allows steering of the antenna pattern within the $-90° < \theta_A < +90°$ range without the presence of grating lobes. At endfire ($\theta_A = \pm 90°$), however, there will be two endfire main lobes. If system design requires that the pattern be steered to endfire, reduction of the d/λ ratio to slightly less than 0.5 will suppress the unwanted grating lobe.

To be completely accurate, the antenna pattern is not only proportional to its array factor, but also to the individual element pattern. When this factor is considered, the result is that equation (3-26) is overly restrictive. The element pattern may attenuate the far out grating lobe in practice to the point that it can be tolerated in visible space. Thus, in an actual antenna array, a ratio of $d/\lambda = 0.5$ is sufficient even at endfire.

Then, assuming this optimum antenna element spacing, the expression for the antenna scan angle in equation (3-23) becomes:

$$| \sin \theta_s | = \frac{4\Delta f \, b}{v} \qquad (3\text{-}27)$$

3.3 System Design and Modeling

When designing a two-beam interference feed such as OFEED for a phased array antenna, the maximum scan angle required by the particular application must first be established. The transmitting frequency must also be known. Then the devices in the feed subsystem can be selected to satisfy these requirements. As with any system, this one is not without limitations.

3.3.1 General Specifications of Devices

The components required in OFEED, shown in Figure 3.1, are: Bragg cell, lasers, AO deflectors, fibers, and detectors. The Bragg cell, maintaining a difference frequency between the two interfering laser beams, is chosen to operate at the desired antenna frequency. The detectors may be PINs or APDs (avalanche photo-diodes). APDs are employed when gain amplification is needed. The remaining devices are appropriately selected to satisfy equation (3-27) (the maximum antenna scan angle requirement).

Inherent to (3-27), the antenna element spacing is 0.5 wavelength. This spacing will accomodate scan angles up to endfire without appearance of an undesired grating lobe. The development of this equation revealed that the scan angle is not dependent on the optical wavelength, L. Thus, the operating wavelength of the lasers is not critical. However, the two lasers must have the same wavelength so that the Bragg cell frequency will be the antenna operating frequency. The lasers of primary interest in fiber systems emit in the 0.8 to 0.9 and 1.3 micrometer spectral regions where transmission losses are minimal [19].

Examination of (3-27) reveals that the scan angle is dependent upon the AO bandwidth (Δf) and the acoustic velocity (v) of the AO deflectors, as well as the fiber spacing (b). The fiber spacing is somewhat flexible, provided it is not less than the diameter of the type of fiber being used. If multimode fiber is used, the spacing

must exceed 50 micrometers. If single mode fiber is used, the spacing can be less. Since the most of the energy is in the beam center, the fiber spacings should be as close as physically possible for higher coupling efficiency.

Acoustic velocities, v in equation (3-27), for AO modulators typically run in the 3 to 7 kilometers/second range for optical wavelengths in the 0.63 to 1.6 micrometer range. The bandwidth of these devices varies and is a function of the center frequency of the device. This center frequency, where optimum performance occurs, is determined by the structure and material. The general relationship between the center frequency and the bandwidth is [20]:

$$f_c \geq 1.5\Delta f \qquad (3\text{-}28)$$

For typical AO deflectors, the bandwidth is below 50 MHz. There are, however, wide bandwidth devices available with bandwidths over a gigahertz. Some data sheets are presented in Appendix B. For the purpose of the optical feed system, typical AO deflectors are adequate.

Thus, design of the optical feed subsystem involves choosing a fiber type, examining AO deflector data sheets, and juggling the values b, Δf, and v to find a fit that will satisfy the particular scan angle requirements.

3.3.2 Computer Modeling

A Fortran program, "FEED", was designed to analyze the optical feed subsystem. The code is presented in Appendix C. It prompts the user for the following inputs:

AO bandwidth being scanned

Acoustic velocity

Optical wavelength of lasers

Fiber spacing

Number of antenna elements

Type of elements

The program assumes 0.5 wavelength spacings of the antenna elements. It then calculates and outputs the following:

Optical interference scan angle

Fiber positions

Antenna element positions along the z-axis

Phases resulting from the interference pattern

Predicted antenna scan angle

A file is created by the program that is suitable for input to the "ARRPAT" [21] program. This program computes the radiation pattern of an antenna array, given the element positions, phases, and type. Thus, for a particular optical feed, the resulting antenna pattern is determined by running these two programs. [Note: There is a convention difference between the equations developed in the above sections and ARRPAT. As defined in the text above, the angle θ is

with respect to the array normal; ARRPAT defines θ as the angle with respect to the array axis.]

3.3.3 Example System

OFEED was experimentally tested by NRL in 1987 [13]. A configuration simulating this experiment was modeled using FEED. The feed system used 830 nanometer lasers, a Bragg cell operating at 3.2 GHz, 50 micrometer core fiber, and AO deflectors with a maximum bandwidth of 30 MHz. The antenna was a linear, equally spaced, seven-element array. The parameters not given in the paper are determined by examining AO deflector data sheets. The assumptions are:

Acoustic velocity = 6 km/s

AO bandwidth scanned = variable depending on the desired antenna scan angle

Fiber spacing = 125 micrometers

3.3.3.1 Broadside Beam

The only experimental datum presented in [13] was for a broadside beam. The resulting rectangular-dB pattern appears in Figure 3.8. As a starting point, this system was modeled using FEED. Figure 3.9 presents the program inputs and outputs. Note that the AO bandwidth is not scanned when a broadside beam is desired. The outputs were then used by ARRPAT to plot the resulting rectangular-linear antenna

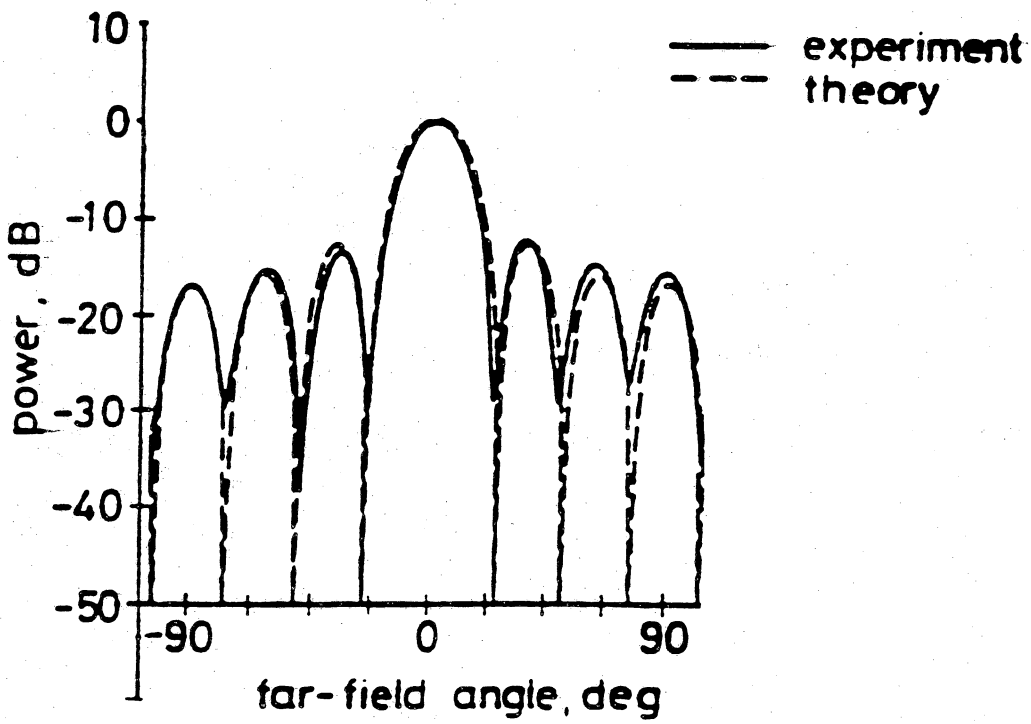

Figure 3.8 NRL experimental results: broadside beam [13].

```
AO BANDWIDTH IN MHZ = 0.

AO VELOCITY IN M/S = 6000.

OPTICAL WAVELENGTH IN NANOMETERS = 830.

FIBER SPACING IN MICROMETERS = 125.

NUMBER OF ELEMENTS IN ARRAY = 07

ISOTROPIC (0) or HALF-WAVE DIPOLES (2) ? 0


OPTICAL INTERFERENCE ANGLE (DEG) =      .0000

 ANTENNA ELEMENT SPACINGS ARE ASSUMED TO BE HALF WAVELENGTH.

 CALCULATED GEOMETRY AND PHASES

    .0000      .0000    -1.5000     1.0000      .0000
    .0000      .0000    -1.0000     1.0000      .0000
    .0000      .0000     -.5000     1.0000      .0000
    .0000      .0000      .0000     1.0000      .0000
    .0000      .0000      .5000     1.0000      .0000
    .0000      .0000     1.0000     1.0000      .0000
    .0000      .0000     1.5000     1.0000      .0000

 MAXIMUM ANTENNA SCAN ANGLE (DEGREES) =      .0000

 THIS ANGLE IS WITH RESPECT TO ARRAY NORMAL.
```

Figure 3.9 FEED inputs and outputs for broadside antenna beam.

pattern. This plot, Figure 3.10, agrees with NRL's experimental data, indicating accuracy of the code and model. Of particular significance are the near-ideal 13 dB sidelobe levels.

3.3.3.2 Scanning the Beam

Scanning the AO frequency results in a proportional antenna beam scan. Using the same system configuration, the only variable input to the FEED program is the AO scan bandwidth. For bandwidths of 3.1 MHz, 6.0 MHz, and 10.4 MHz, the antenna scans 15°, 30°, and 60°, respectively. The results are presented in Figures 3.11 through 3.16. The accuracy of the interelement phase shift is ideal, indicating perfect microwave phase control.

3.3.4 Design Improvements

Depending on the particular application, the example system design can be improved to accomodate more stringent requirements.

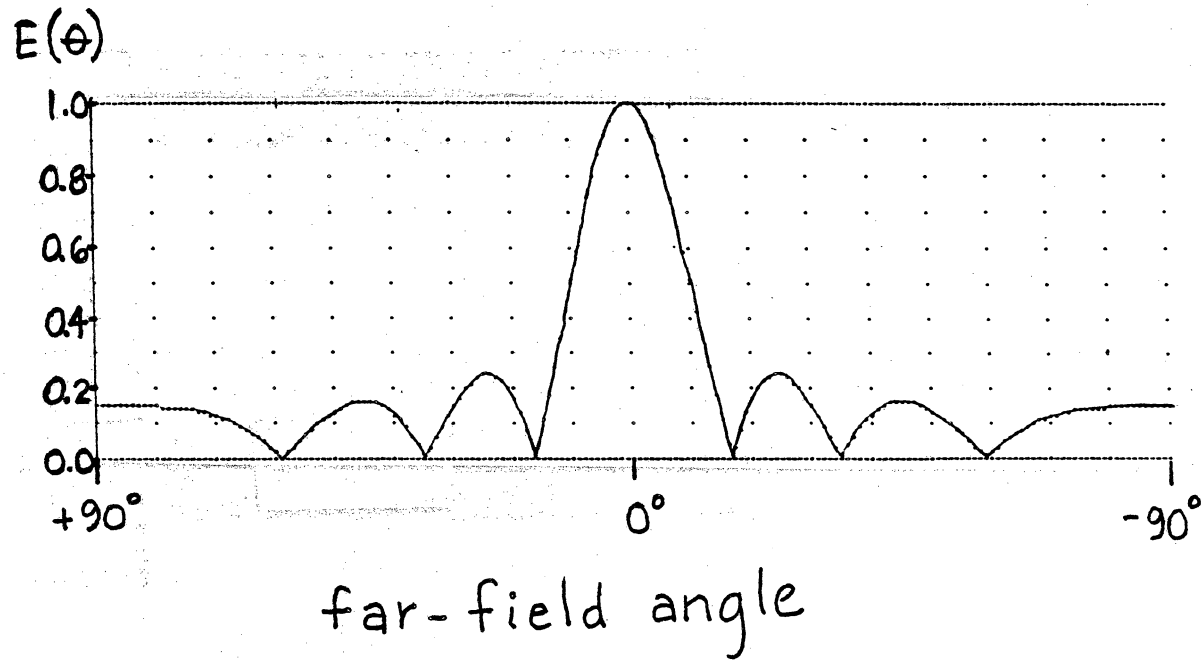

Figure 3.10 ARRPAT rectangular plot resulting from Figure 3.9 FEED outputs. Broadside beam.

```
AO BANDWIDTH IN MHZ = 3.105829

AO VELOCITY IN M/S = 6000.

OPTICAL WAVELENGTH IN NANOMETERS = 830.

FIBER SPACING IN MICROMETERS = 125.

NUMBER OF ELEMENTS IN ARRAY = 07

ISOTROPIC (0) or HALF-WAVE DIPOLES (2) ? 0


OPTICAL INTERFERENCE ANGLE (DEG) =      .0492

 ANTENNA ELEMENT SPACINGS ARE ASSUMED TO BE HALF WAVELENGTH.

 CALCULATED GEOMETRY AND PHASES

    .0000      .0000    -1.5000     1.0000 -139.7623
    .0000      .0000    -1.0000     1.0000  -93.1749
    .0000      .0000     -.5000     1.0000  -46.5874
    .0000      .0000      .0000     1.0000     .0000
    .0000      .0000      .5000     1.0000   46.5874
    .0000      .0000     1.0000     1.0000   93.1749
    .0000      .0000     1.5000     1.0000  139.7623

 MAXIMUM ANTENNA SCAN ANGLE (DEGREES) =   15.0000

 THIS ANGLE IS WITH RESPECT TO ARRAY NORMAL.
```

Figure 3.11 FEED inputs and outputs for 15° antenna scan angle.

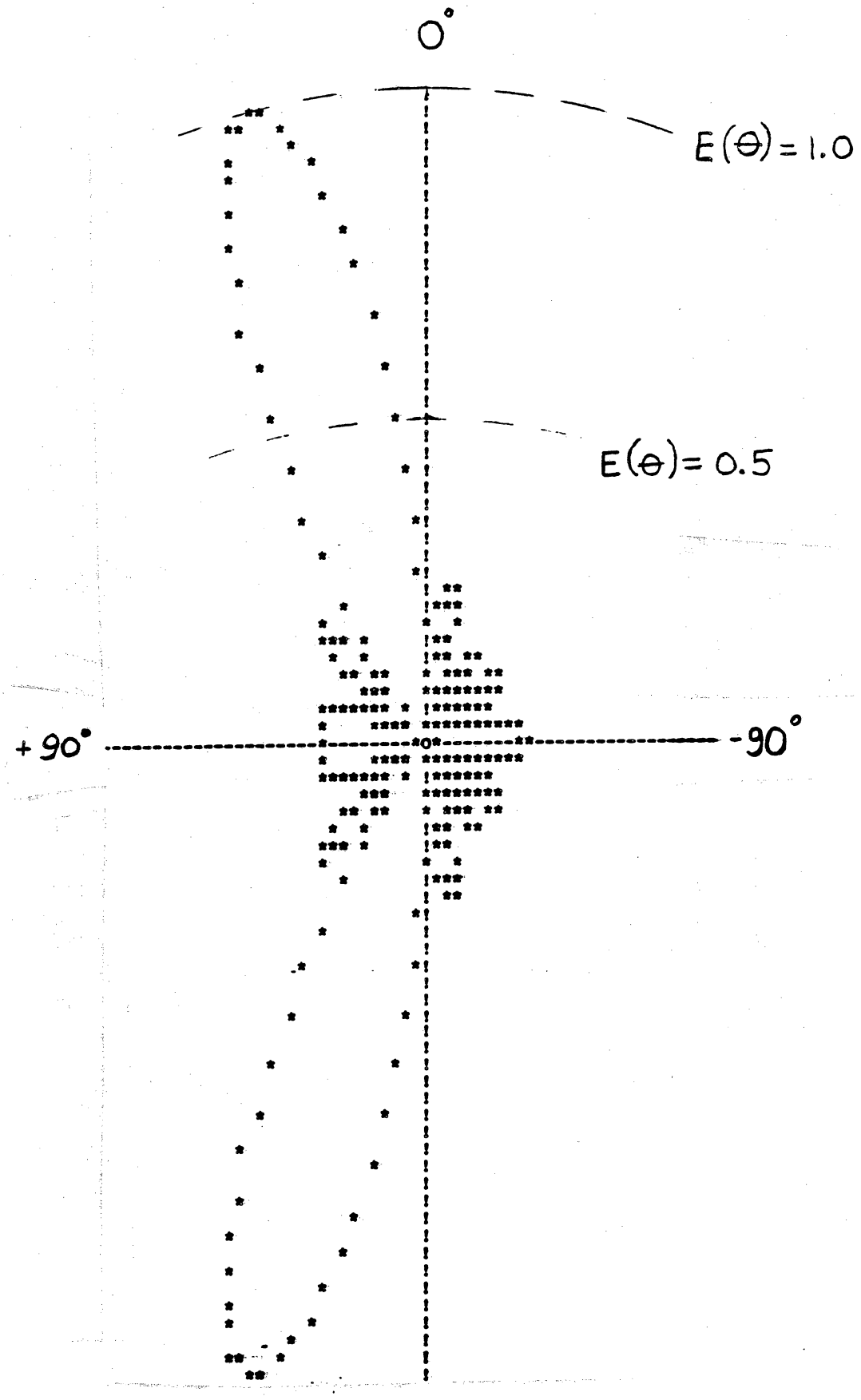

Figure 3.12 ARRPAT polar plot resulting from Figure 3.11 FEED outputs. Resulting scan angle = 15°.

```
AO BANDWIDTH IN MHZ = 6.0

AO VELOCITY IN M/S = 6000.

OPTICAL WAVELENGTH IN NANOMETERS = 830.

FIBER SPACING IN MICROMETERS = 125.

NUMBER OF ELEMENTS IN ARRAY = 07

ISOTROPIC (0) or HALF-WAVE DIPOLES (2) ? 0


OPTICAL INTERFERENCE ANGLE (DEG) =      .0951

 ANTENNA ELEMENT SPACINGS ARE ASSUMED TO BE HALF WAVELENGTH.

 CALCULATED GEOMETRY AND PHASES

    .0000      .0000    -1.5000     1.0000 -270.0000
    .0000      .0000    -1.0000     1.0000 -180.0000
    .0000      .0000     -.5000     1.0000  -90.0000
    .0000      .0000      .0000     1.0000     .0000
    .0000      .0000      .5000     1.0000   90.0000
    .0000      .0000     1.0000     1.0000  180.0000
    .0000      .0000     1.5000     1.0000  270.0000

 MAXIMUM ANTENNA SCAN ANGLE (DEGREES) =   30.0000

 THIS ANGLE IS WITH RESPECT TO ARRAY NORMAL.
```

Figure 3.13 FEED inputs and outputs for 30° antenna scan angle.

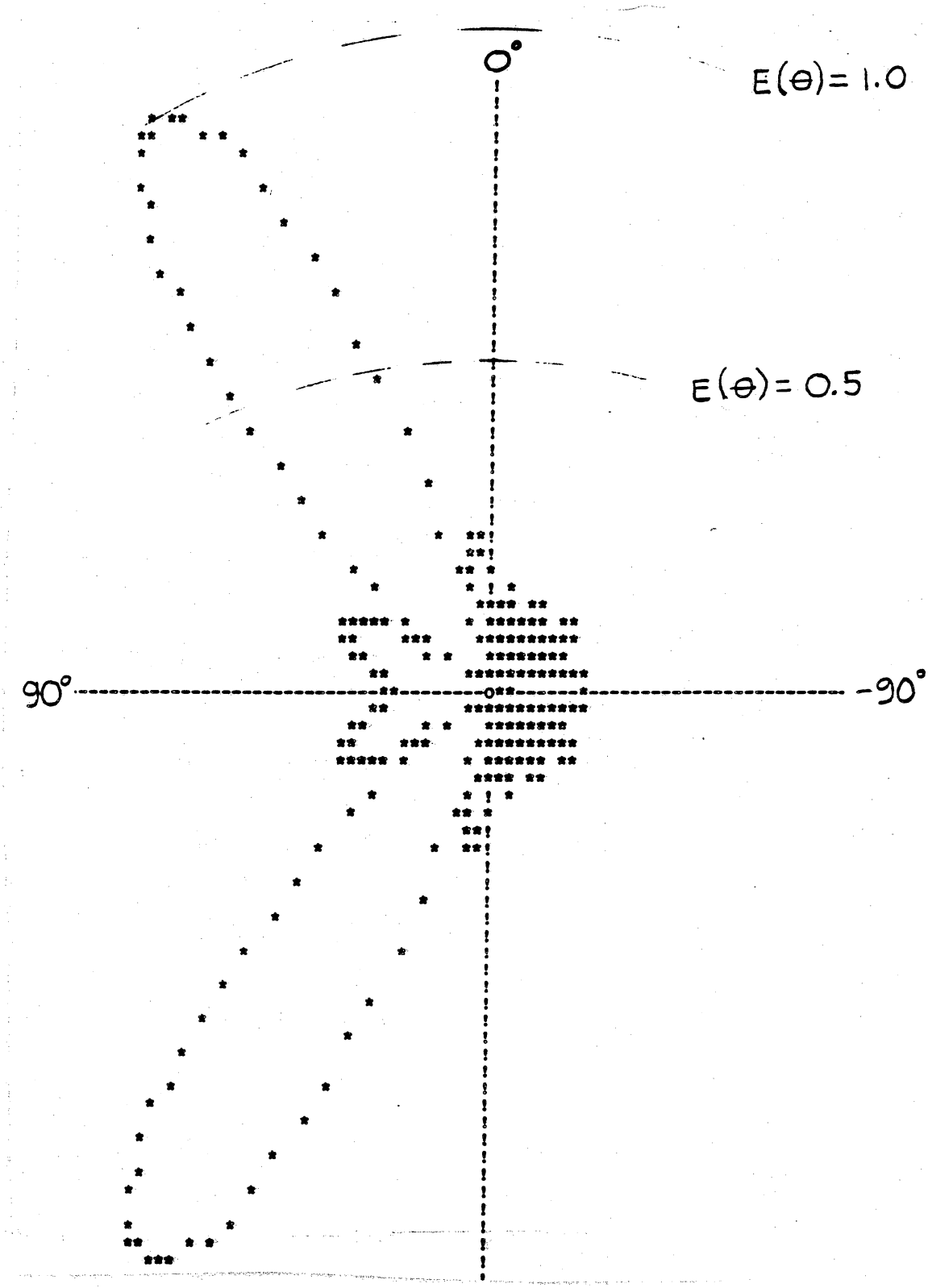

Figure 3.14 ARRPAT polar plot resulting from Figure 3.13 FEED outputs. Resulting scan angle = 30°.

```
AO BANDWIDTH IN MHZ = 10.3923

AO VELOCITY IN M/S = 6000.

OPTICAL WAVELENGTH IN NANOMETERS = 830

FIBER SPACING IN MICROMETERS = 125.

NUMBER OF ELEMENTS IN ARRAY = 07

ISOTROPIC (0) or HALF-WAVE DIPOLES (2) ? 0


OPTICAL INTERFERENCE ANGLE (DEG) =      .1647

 ANTENNA ELEMENT SPACINGS ARE ASSUMED TO BE HALF WAVELENGTH.

 CALCULATED GEOMETRY AND PHASES

    .0000      .0000    -1.5000     1.0000 -467.6536
    .0000      .0000    -1.0000     1.0000 -311.7690
    .0000      .0000     -.5000     1.0000 -155.8845
    .0000      .0000      .0000     1.0000     .0000
    .0000      .0000      .5000     1.0000  155.8845
    .0000      .0000     1.0000     1.0000  311.7690
    .0000      .0000     1.5000     1.0000  467.6536

 MAXIMUM ANTENNA SCAN ANGLE (DEGREES) =   60.0000

 THIS ANGLE IS WITH RESPECT TO ARRAY NORMAL.
```

Figure 3.15 FEED inputs and outputs for 60° antenna scan angle.

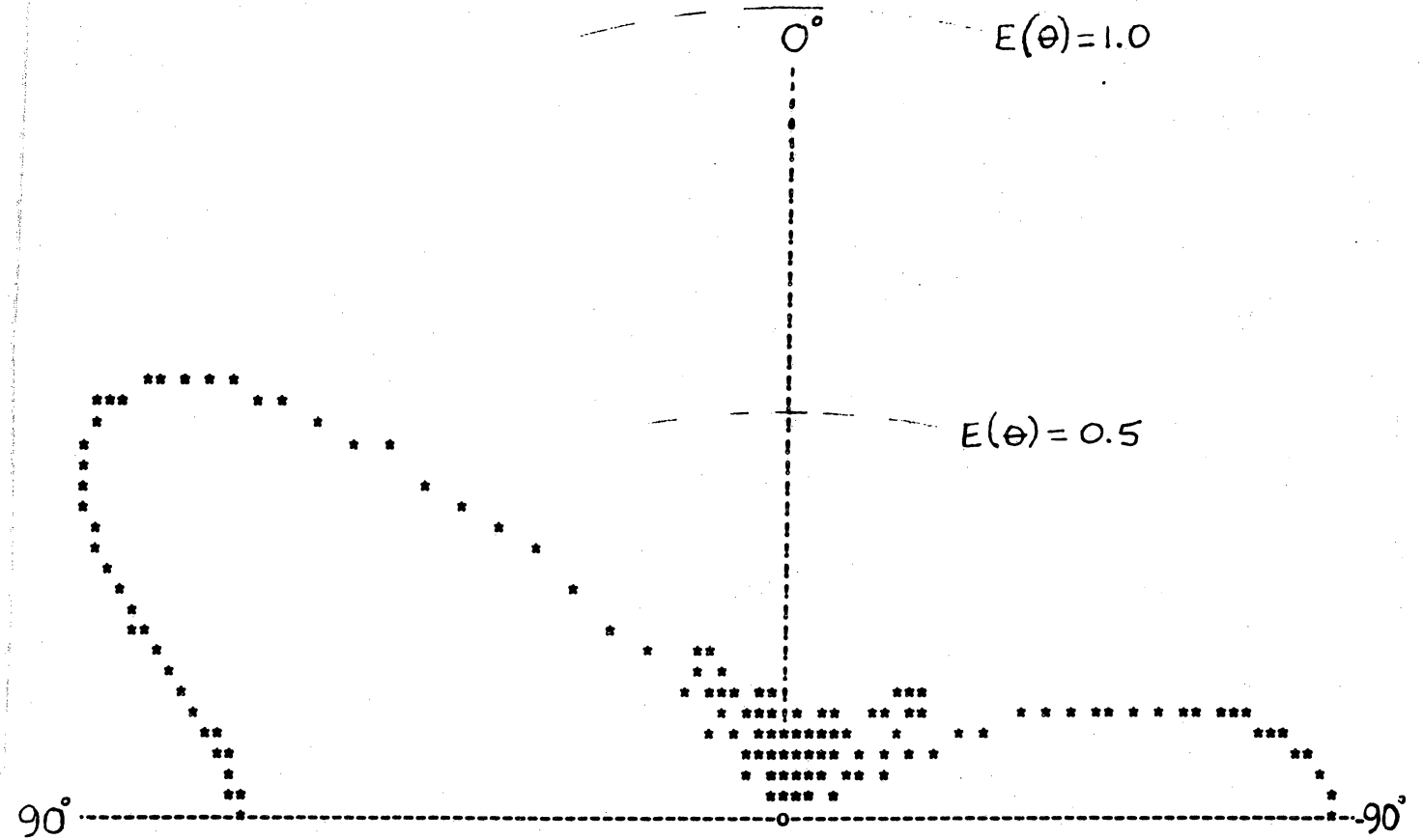

Figure 3.16 ARRPAT polar plot resulting from Figure 3.15 FEED outputs. Resulting scan angle = 60°.

3.3.4.1 Narrower Beamwidth

The half-power beamwidth is a function of both the array length and the beam pointing angle. Improvements in this area involve making changes in the antenna design. For a given array length, the beamwidth increases as the angle is scanned off broadside. The array length is defined by the product Nd, where N is the number of elements and d is the element spacing. Increasing this product narrows the beamwidth. However, increasing the spacing, d, can cause the appearance of undesired grating lobes as discussed in section 3.2.6. Thus, to reduce the beamwidth without causing grating lobes, the number of elements is increased.

In the plot of Figure 3.17, the beam is scanned to 60° with the number of elements increased to 15. Compare the improved narrow beamwidth pattern with that of Figure 3.16 where the number of elements is 7.

3.3.4.2 Lower Sidelobe Levels

In many applications, the sidelobe level is critical and must be maintained at very low levels, i.e. 30 dB or less. The sidelobe levels can be controlled by adjusting the amplitudes of the currents in an array. Techniques such as Dolph-Chebyshev and Tapered Taylor weightings are presented in [18] and [21] for determining the appropriate array excitations for given sidelobe levels. In essence, these

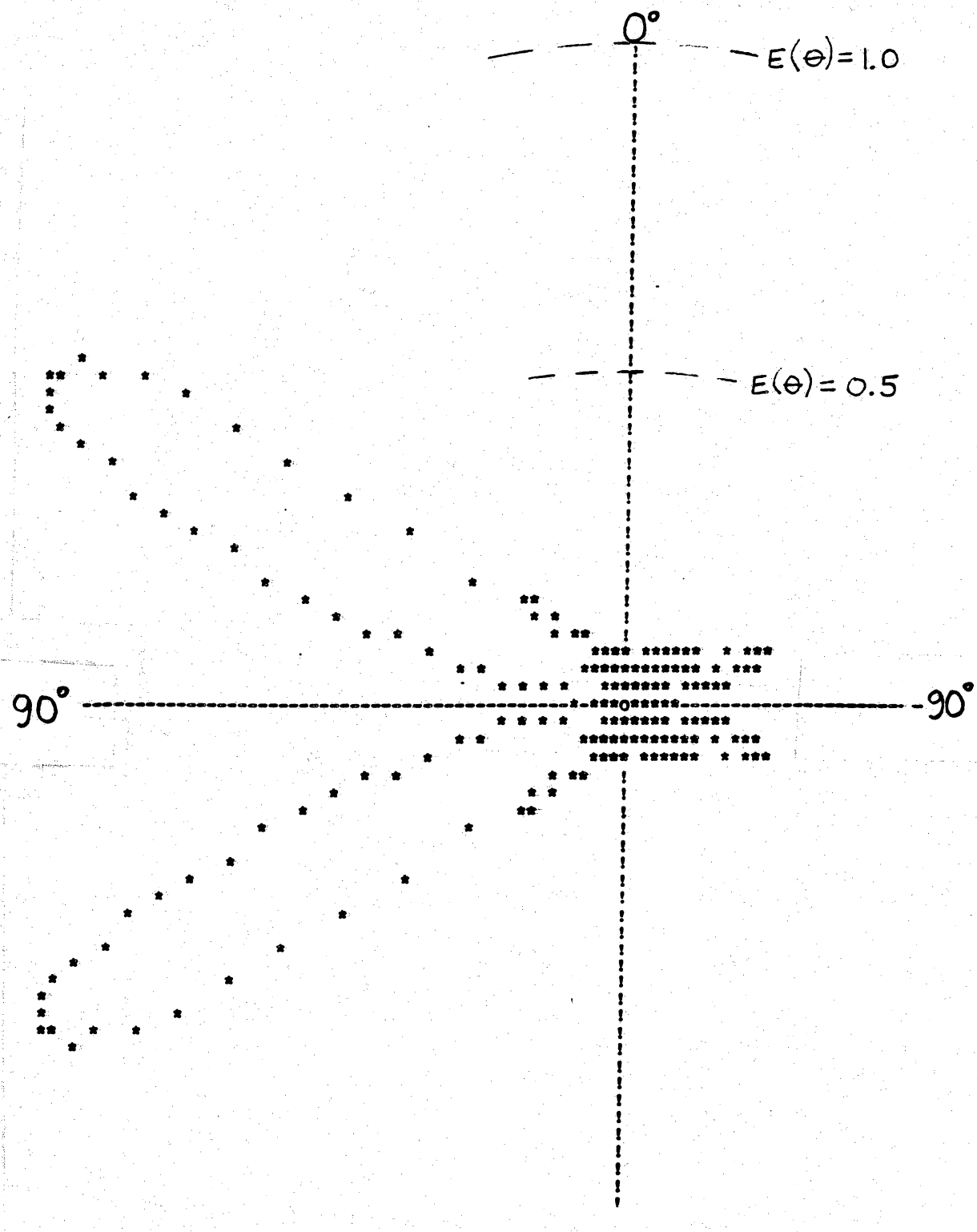

Figure 3.17 ARRPAT polar plot for 60° scan angle; 15 elements.

techniques taper the distribution such that the largest excitation occurs at the center of the array.

In the OFEED configuration, a cylindrical lens is placed in front of the fiber array for improved coupling and equal illumination. It is possible to insert an array of optical attenuators in such a way as to create a tapered distribution. Another alternative in the case of APD detectors is to adjust their gains in a tapered manner across the array. The other method is to insert an array of traditional variable gain amplifiers between the detectors and the antenna elements to create the desired tapered excitation.

It is important to note that lower sidelobe levels are not obtained without a sacrifice. The resulting patterns have increased beamwidths and reduced directivity. However, careful design can optimize the tradeoff.

3.3.4.3 Fiber Selection

From an efficiency standpoint, single mode fibers may be preferrable to multimode fibers. The optical mixing that occurs in the detectors is very sensitive to the phase-front and amplitude cross section of the two interfering light beams. For high mixing efficiency, a close match of the beam diameters and phase-front curvatures at the photodetector surface is necessary. The use of single mode fibers greatly simplifies this alignment because both waves exit from the

fiber perfectly matched [12]. Thus the gain required by the system is further reduced.

Multimode interferometers are generally less sensitive due to the fact that each mode may be considered as a reference for any one of the other modes. Thus, distortion in the demodulated output may occur caused by the random relative phases of the interfering modes. Even so, acceptable performance is attainable with a multimode system due to the inherent high sensitivity of interferometers.

Another advantage of using single mode fibers in OFEED is the increased number of elements that can be accomodated. Single mode fibers are much smaller and thus many more can fit in a given area. Further discussion on this aspect is presented in section 3.3.5.2.

The selection of single mode or multimode will depend on the particular power requirements, resolution requirements, and the number of elements in the system. Single mode fiber provides improved efficiency, higher sensitivity, and accomodates more elements.

3.3.4.4 A Receiving Antenna Design

For a receiving antenna, the same OFEED subsystem can be used to discriminate between signals from different directions. Figure 3.18 shows the modified system with the only addition being an array of RF mixers [12]. The frequency difference between the two light waves provides a

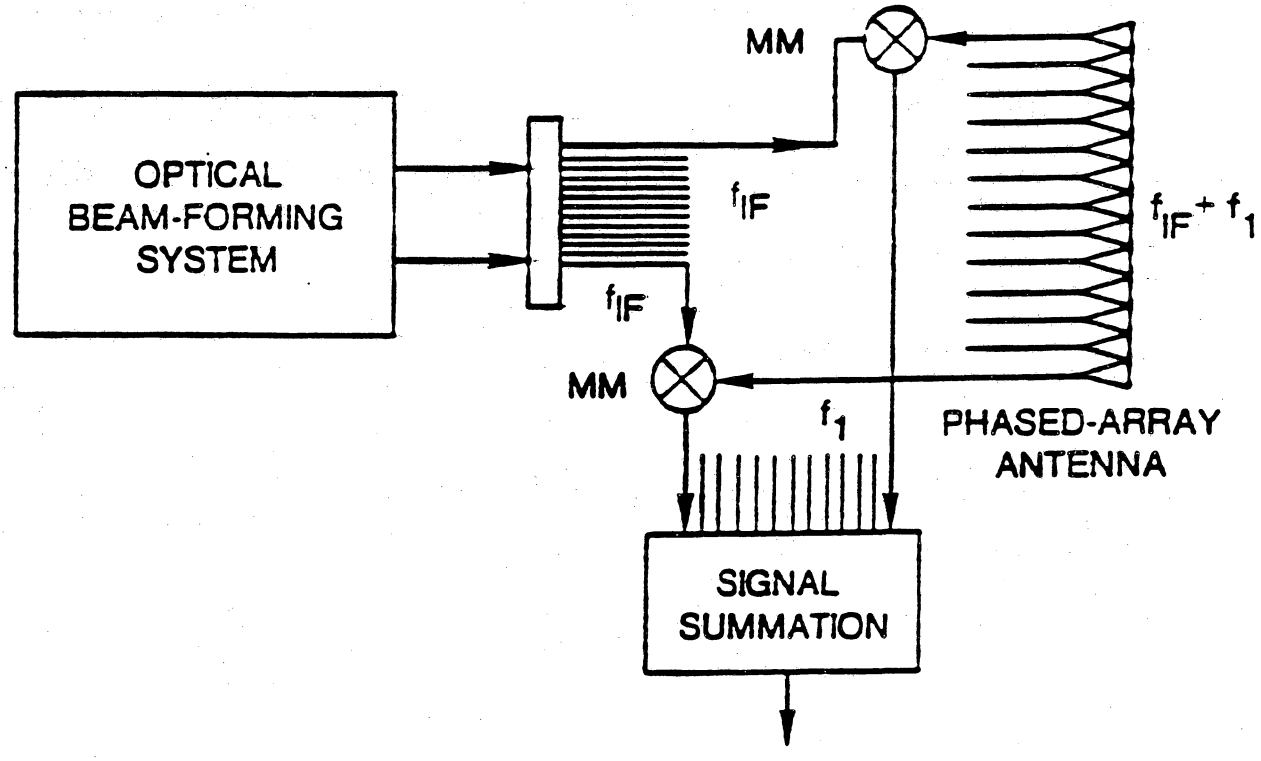

Figure 3.18 Receiving optical/microwave antenna design [12].

convenient second intermediate frequency at the output of the RF mixers. The directional information of a received wave is contained in a phase ramp across the aperture of the array because of the difference in arrival time at the elements. At the output of the array of mixers, all the signals are coherent if a phase ramp of equal depth but opposite sign is generated in the optical subsystem. A summation of these signals is then possible. Signals that are in the same frequency band but from other directions have variable phases and suffer partial cancellations in the summation process. Thus, in such a system, the optical feed functions as a matched filter.

3.3.4.5 Scanning Azimuth and Elevation

With a few modifications, OFEED can be made to scan in both azimuth and elevation. This requires that two AO deflectors be mounted orthogonally in each leg of the system to provide XY scan capability. Alternatively, there are dual axis deflectors (such as the LS110-XY) commercially available to serve this function. Appendix B contains data sheets on these devices.

3.3.5 Limitations and Alternatives

The system limitations are discussed and possible alternatives suggested.

3.3.5.1 Operating Frequency

The most obvious limitations in the current system configuration involve the Bragg cell which is used to establish the microwave frequency. The maximum frequency shift attainable with Bragg cells is around 4 GHz. This was achieved in a laboratory model using very narrow beam diameter lasers operating in the 830 nanometer region [22]. As a result of shorter acousto-optic interaction length at higher frequencies, Bragg cell design encounters low loss material availability, high acoustic power density, and smaller optical diffraction efficiency. Several efficiency enhancement techniques are being investigated, and it is expected that devices with up to 10 GHz center frequencies will be possible in the near future [20]. Until that time, there are other alternatives for establishing an operating frequency greater than this 3 to 4 GHz limit.

One possible approach is to cascade several Bragg cells to obtain the desired frequency shift. However, examination of the efficiencies of cells in the GHz range makes this alternative not viable.

Another possibility would be to perform the optical beam

forming at an intermediate frequency, i.e. an available Bragg cell frequency. While this is a viable method, it would require upconverters at each antenna element and further complicate the system.

Actually, if the desired operating frequency is 10 GHz or less, an external modulating scheme such as a Bragg cell is not necessary. Direct modulation of semiconductor lasers has been demonstrated at frequencies exceeding 10 GHz [23]. This development allows for a simpler design in that a single laser can be used in combination with a beam splitter to create the two beams necessary. As a further improvement, a surface-acoustic-wave (SAW) cell can be used in place of the AO modulators to steer the beam. SAW cells can accomodate two transducers [24] which does away with the need for the interferometric structure. Two oppositely directed acoustic waves are thus generated in the same cell to modulate signal and reference beam, respectively. Figure 3.19 presents the alternative system configuration.

At operating frequencies above the 10 GHz range, external modulation of the lasers is inevitable. The frequency synchronization can be achieved by optical injection locking of local oscillators. As early as 1984, a 17 GHz integrated-optic modulator was demonstrated [26]. With more research efforts being devoted to the high frequency links, the possibilities are improving. Indirect optical injection locking techniques are currently receiving much of this effort [27]. Impatt oscillators at 39 GHz have been locked using this method [28]. The basis for the technique is that

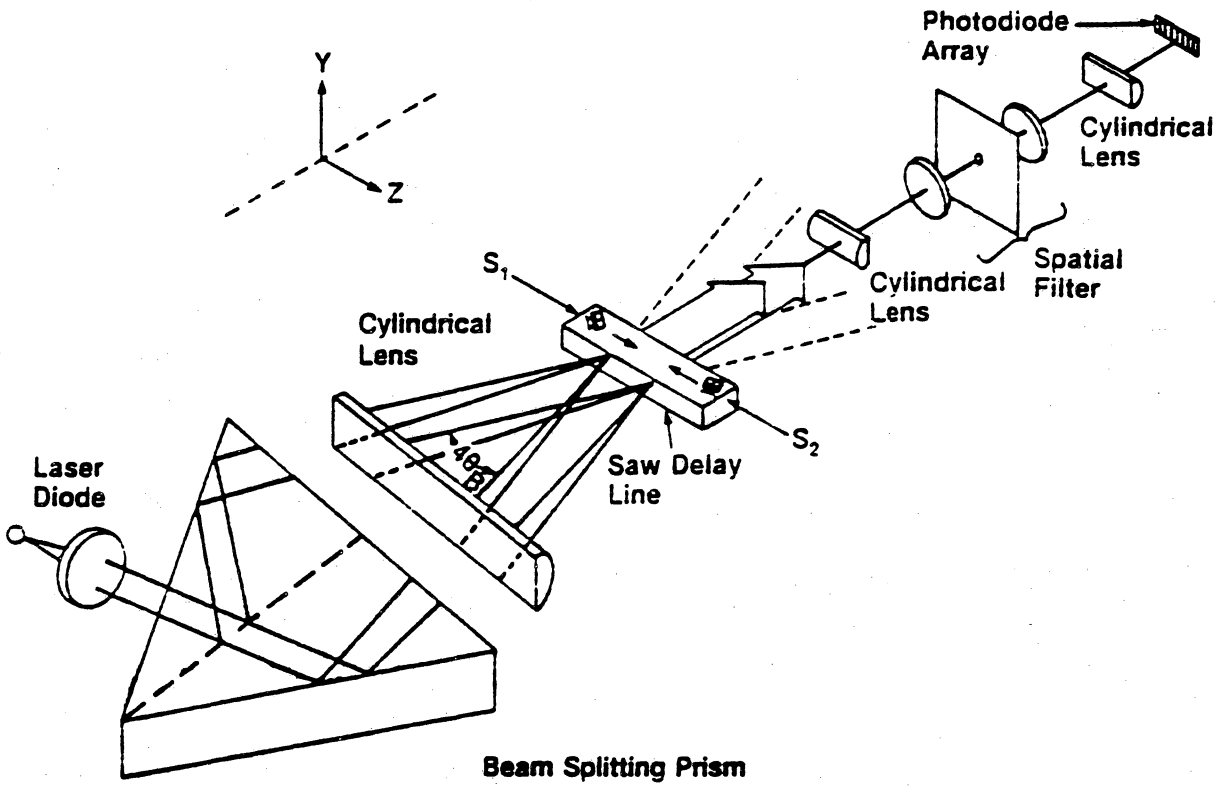

Figure 3.19 Improved optical feed using a single laser and SAW modulators [25].

large-signal modulation of lasers provides higher order harmonics of the modulating frequency and thereby extends the effective bandwidth. In order to obtain frequency sychronization at even higher frequencies, optical feedback is being investigated to increase the possible modulation depths.

With the availability of the 10 GHz bandwidth laser, the optical injection locking of oscillators in the 60 to 90 GHz communication bands becomes a distinct possibility.

3.3.5.2 Number of Elements

The number of elements that can be accomodated by the OFEED system of Figure 3.1 depends on the array geometry and the size and spacing of the fibers. The two-beam optical interference pattern can be imaged onto the fiber array with different magnifications using an appropriate lens. Depending on how much of the two-beam interference pattern is used to illuminate the fiber array, a larger or smaller band of spatial frequencies is transmitted to the array. For better efficiency, practical systems will use only the central fringe of the pattern.

The width of this central fringe can be magnified by optimally placing a lens of focal length F in front of the fiber array. The resulting spread is proportional to the F/D ratio, where D is the fringe diameter at the AO deflector output. The new fringe diameter is defined by:

$$D' = 2 L F / D \qquad (3\text{-}29)$$

where L is the optical wavelength. A central fringe width of several millimeters is easily obtained with a 10 centimeter focal length lens.

Using this criterion for maximum efficiency, the fiber array must be spaced such that it fits in a length of a few millimeters. Consider the linear array example system of section 3.3.3 and assume the central fringe diameter at the AO deflector output is 50 micrometers. If a 10 centimeter focal length lens is used, then the resulting fringe width becomes 3.32 millimeters. Thus the fiber array must fit in a 3.32 millimeter length. If the same fiber spacing of 125 micrometers is employed and the fibers are arranged linearly, the system will accomodate up to 26 elements. Alternatively, if single mode fibers are used with 25 micrometer spacings, 132 elements can be allowed.

However, fibers can be packed much more densely in a bundle rather than in a line. Thus, if the antenna array is planar (circular or rectangular), many more elements can be accomodated since the fibers must fit in an area of several millimeters rather than a length. With proper choice of the lens, thousands of fibers can be arranged in an array occupying the resulting fringe area.

3.3.5.3 Scan Time

The time required to alter the microwave phase angle is referred to as the scan time. With rapid beamsteering being an important goal of the phased-array antenna, it is necessary to analyze the OFEED subsystem in terms of its scan time capabilities. The phase controllers in the system are the AO deflectors and their scan times are determined by their time apertures.

The time aperture of a cell is a measure of the time available for sound and light to interact, and it depends largely on the rate at which the cell material attenuates the acoustic wave [29]. For large bandwidth cells, the interaction length is shorter and thus the time aperture is smaller. Scan times as low as 100 nanoseconds are available in bulk AO deflectors, and times less than 10 nanoseconds have been obtained with SAW cells. In lower bandwidth deflectors (<500 MHz), the smallest time aperture is on the order of a few microseconds for bulk devices and a few hundred nanoseconds for SAW cells.

When the antenna is functioning as a correlator, it must transform the difference in arrival times between a pair of signals into a position (Figure 3.18). For this application, the desired AO deflector time aperture is large to handle long relative delays. Commercially available devices have time apertures as large as 80 microseconds; and time apertures as long as 150 microseconds have been demonstrated experimentally.

CHAPTER 4. CONCLUSIONS

The underlying purpose of this thesis is to determine the optimum design of an optical feed for phased array antennas. To accomplish this, a critical survey of optical technologies for feeding phased arrays is conducted. The benefits of an optical implementation versus the conventional implementation are assessed. An overview of current research efforts is presented and evaluated. The practicalities and limitations are determined for each proposed method. Table 4.1 summarizes this effort.

The evaluation shows the two-beam interference method (OFEED) to be superior to other optical feed systems. Because of its technically unique and simple design, only a handful of components is required to feed a large antenna array. The theory of operation is derived which involves Bragg diffraction, the interference of two coherent light beams, some basic phased array antenna theory, and the optical-to-microwave phase correlation. Based on this theory, a computer model is developed to analyze the optical feed subsystem. An example system is analyzed and the resulting antenna radiation patterns are found to be ideal. Some design improvements are suggested that will allow OFEED to accommodate a broad range of applications including: scan capability in both azimuth and elevation, narrow

beamwidth and low sidelobe level requirements, increased efficiency, and receiving antenna implementation.

The optimum system, OFEED, is also analyzed in terms of its limitations. The maximum operating frequency is determined and some design alternatives are suggested that extend the limit up to 40 GHz using existing, proven technology. Research in this area indicates that operation in the 60 to 90 GHz bands is a distinct possibility. The number of antenna elements that OFEED can accomodate is found to be in the thousands, which is quite adequate. The scan time capability of OFEED is dependent upon the bandwidth of the AO devices. Commercially available devices exhibit maximum and minimum scan times of 80 microseconds and less than 10 nanoseconds, respectively.

While OFEED does possess limitations (what system doesn't?), there are three important conclusions to draw: 1) as is, the system will accomodate many applications for phased array antennas; 2) a few design modifications greatly extend its range of applications; and 3) ongoing research is promising to extend its capabilities even further.

Table 4.1 Optical Feed Methods

METHOD	TIME DELAY (T) or PHASE SHIFT (P)	LIMITATIONS
Fiber stretching	T	small phase shifts phase accuracy reliability
Mode coupling	T	cost, complexity
Wavelength varying	T	cost, complexity
Fiber length varying	T	array size accuracy, SNR
Optical injection of semiconductors	P	operating frequency complexity
Interferometer with E/O phase shifter	P	power consumption operating frequency complexity
Original 2 beam interference w/fiber array	P	frequency < 4 GHz scan time > 2 s
Improved 2 beam interference w/fiber array	P	frequency > 40 GHz scan time < 10 ns

APPENDIX A. FAR-FIELD DIFFRACTION THEORY

A standard treatise of far-field diffraction of light is presented in this appendix because of its importance in OFEED. This phenomenon occurs in the AO devices of Figure 3.1. The theory development and figures are taken from references [14] and [15].

The far-field distribution is called the Fraunhofer diffraction pattern and its amplitude is given by the equation:

$$A = C \int e^{ikr} \, dS \qquad (A-1)$$

where

A = the amplitude of the wave

C = a constant incorporating scale factors

k = propagation constant = $2\pi/L$
where L is the wavelength

r = far-field distance

dS = area of elementary section of aperture

Considering a single slit of width w and length l and two parallel rays making an angle θ to the Z axis, the geometry of Figure A.1 results. At some point on the upper ray at a distance r from the slit:

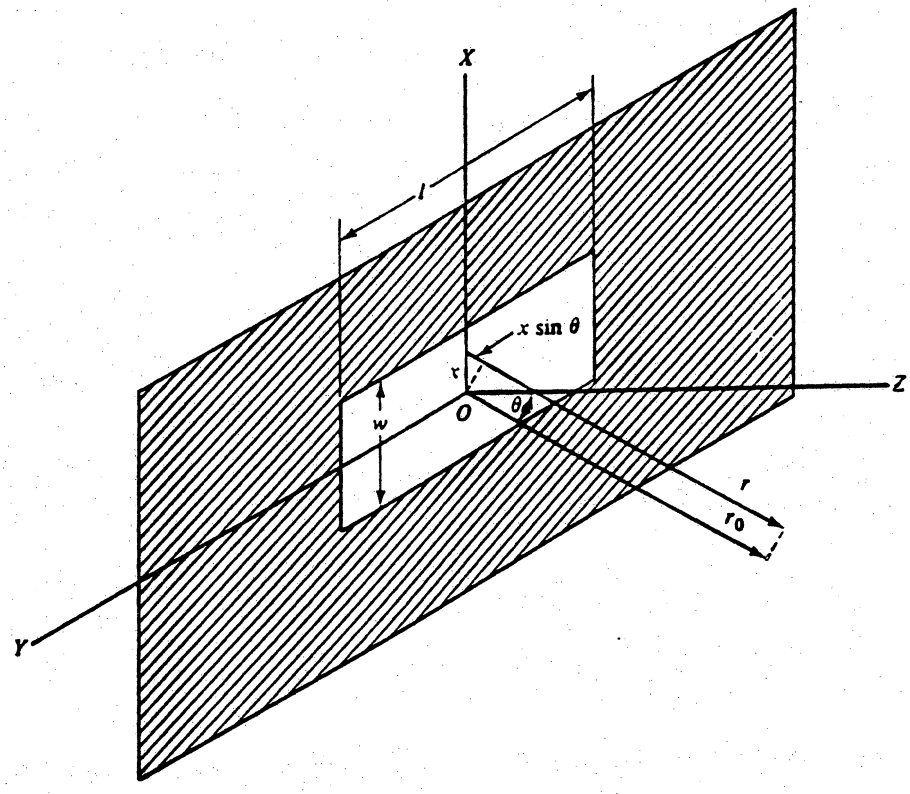

Figure A.1 Geometry of single slit diffraction [15].

$$r = r_o + x \sin\theta \qquad \text{(A-2)}$$

where r_o is the corresponding value of r on the lower ray. The element of area in the slit is:

$$dS = l\, dx \qquad \text{(A-3)}$$

Then the amplitude of the far-field pattern becomes:

$$A = C\, e^{ikr_o} \, l \int_{-w/2}^{w/2} e^{ikx \sin\theta} \, dx \qquad \text{(A-4)}$$

Performing the integration yields:

$$A = C' \operatorname{sinc} \alpha \qquad \text{(A-5)}$$

where

$$C' = C\, e^{ikr_o}\, wl/2$$

$$\operatorname{sinc} \alpha = \sin\alpha/\alpha$$

$$\alpha = \tfrac{1}{2} kw \sin\theta$$

The relative intensity of the far-field pattern is defined to be:

$$I/I_o = \frac{\sin^2\alpha}{\alpha^2} \qquad \text{(A-6)}$$

where

$$I = \tfrac{1}{2} A A^*$$

$$I_o = \tfrac{1}{2} C' C'^* = \text{value of } I \text{ for } \alpha = 0$$

The curve of $(I/I_o) = (\sin\alpha/\alpha)^2$ versus α is plotted in Figure A.2. The principal maximum occurs at $\theta = 0$ ($\alpha = 0$). The minima correspond to $\sin\alpha = 0$ (but $\alpha \neq 0$) which gives:

$$\alpha = m\pi, \qquad m = \pm 1, \pm 2, \ldots \tag{A-7}$$

or

$$\sin\theta = mL/w \tag{A-8}$$

For small angles, $\sin\theta \approx \theta$ and this becomes:

$$\theta = mL/w \tag{A-9}$$

Now in the case of a grating with N lines of width w, spaced at a distance d, the diffraction pattern has been derived as:

$$\frac{I}{I_o} = \text{sinc}^2\alpha \left(\frac{\sin N\Gamma}{N \sin\Gamma}\right)^2 \tag{A-10}$$

where

$$\Gamma = \tfrac{1}{2}\, kd \sin\theta$$

A plot of this pattern (I/I_o versus Γ) is shown in Figure A.3. The function $\text{sinc}^2\alpha$, which defines the envelope of the curve, is known as the shape factor and is due to the individual lines. The other term, $[(\sin N\Gamma)/(N \sin\Gamma)]^2$, is the grating factor and defines the fine structure of the curve. It is due to the spacing of the lines.

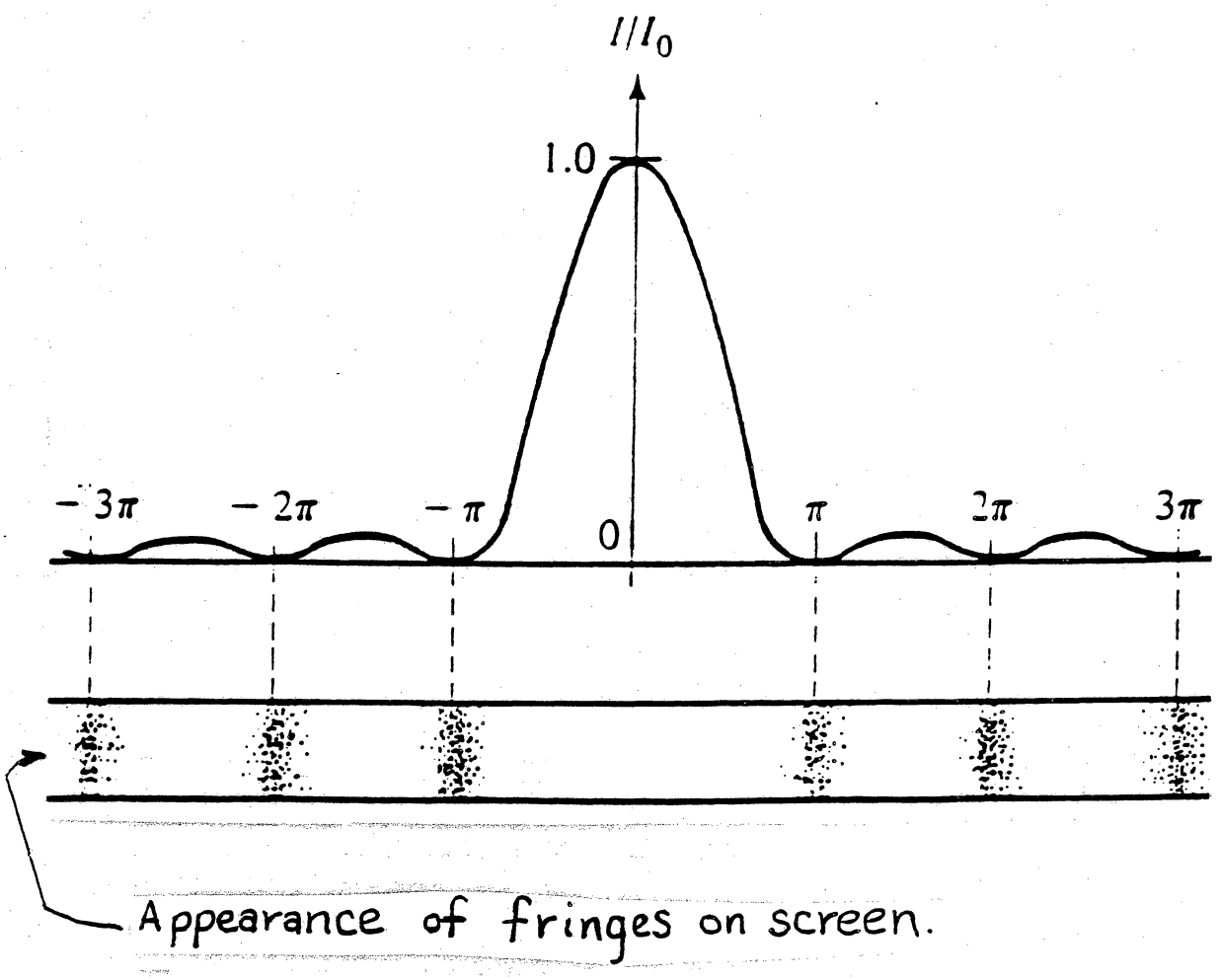

Figure A.2 Curve of (I/I_o) versus α [15].

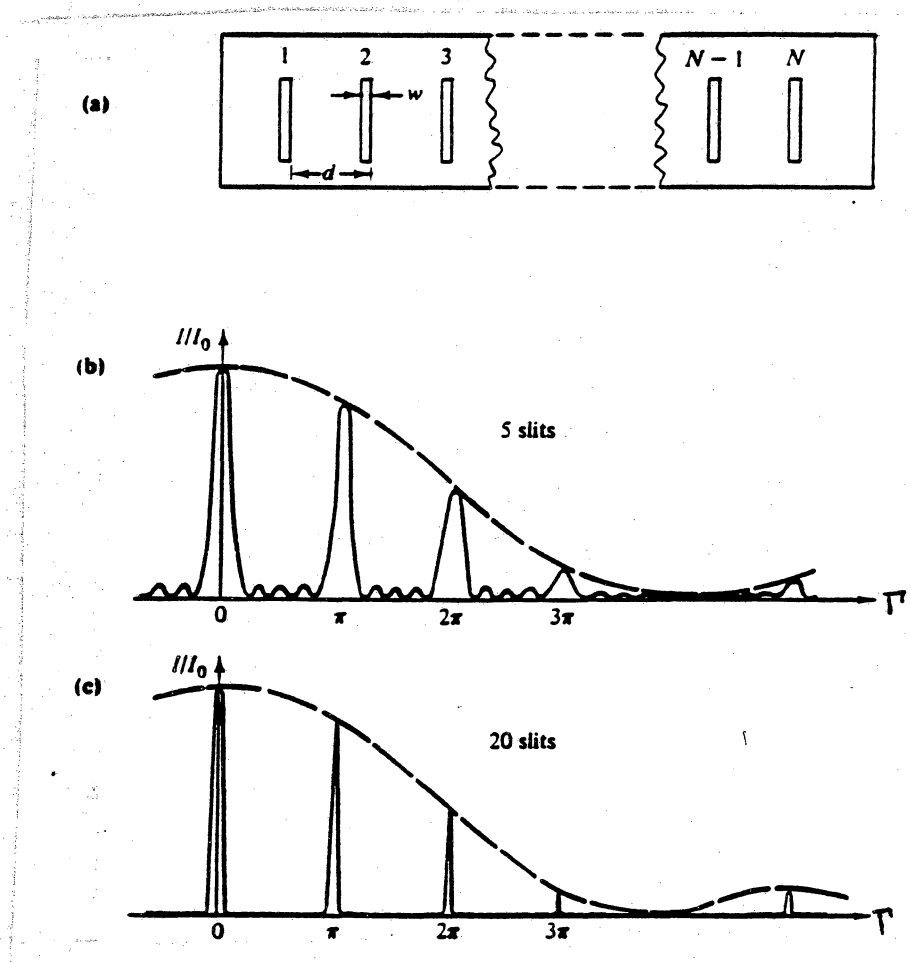

Figure A.3 Curve of (I/I_o) versus Γ for N slits [15].

In comparison with the single slit pattern of Figure A.2, the central lobe of sinc α has been diffracted into a number of sharp maxima such that the grating far-field pattern consists of a large number of very narrow, closely spaced lines. These maxima are called spectra of order m and occur for values of Γ which make the denominator of the grating factor vanish. That is:

$$\Gamma = m\pi \qquad m = 0, \pm 1, \pm 2, \ldots \qquad \text{(A-11)}$$

or, equivalently,

$$\tfrac{1}{2} kd \sin \theta_m = m\pi \qquad \text{(A-12)}$$

where the θ_m are the angles with respect to the normal. Substituting $2\pi/L$ for k, this becomes

$$d \sin \theta_m = mL \qquad \text{(A-13)}$$

Note: More exact diffraction theories contain an obliquity factor in the diffraction integral of equation A-1. However, for small angles, this factor of $(1 + \cos \theta)$ is approximately equal to unity and can be neglected.

APPENDIX B. DEVICE DATA SHEETS

This appendix presents data sheets for commercially available AO deflectors and Bragg cells. The pertinent parameters of acoustic velocity and bandwidth are specified.

MODEL 1205C*

ISOMET

ACOUSTO-OPTIC MODULATOR

July 1986

APPLICATIONS

* Modulator
* Low Resolution Deflector
* Frequency Shifter

FEATURES

* Low Drive Power
* Small Size
* Good Temperature Stability

* 1205C-1 1mm Active Aperture
  1205C-2 2mm Active Aperture

SPECIFICATIONS

Spectral Range	:	.442 - > 1.5μm*
Standard Operating Wavelengths	:	442nm, 488-633nm
Interaction Medium	:	Lead Molybdate ($PbMoO_4$)
Acoustic Velocity	:	3.63mm/μs
Active Aperture	:	1mm and 2mm (See Below)
Center Frequency (CF)	:	80MHz
RF BAndwidth	:	30MHz
Input Impedance	:	50Ω Nominal
VSWR	:	< 1.5:1 @ 80MHz
DC Contrast Ratio	:	> 1000:1

PERFORMACE VS. WAVELENGTH

Wavelength (nm)	: 442	488	515	633	830*
RF Drive Power, 1205C-1 (W)	: <0.3	<0.4	<0.4	<0.6	<0.8
RF Drive Power, 1205C-2 (W)	: <0.4	<0.5	<0.6	<1.0	<1.5
Bragg Angle (mr)	: 4.9	5.4	5.7	7.0	9.1
Beam Separation (mr)	: 9.7	10.7	11.3	13.9	18.3
Static Insertion Loss (%)	: <10	<5	<3	<3	<3

PERFORMANCE VS. BEAM DIAMETER

Beam Diameter (mm)	: 2.0	1.0	0.34	0.2	0.14
Rise Time (ns)	: 360	180	60	35	25
Modulation Bandwidth (MHz) @ MTF = 0.5	: 1	1.9	5.8	10	15
Deflection Efficiency (% @ CF)	: 90	85	85	80	75
T • Δf Product	: 16	11	NA	NA	NA

MODEL LS110-XY

DUAL AXIS ACOUSTO-OPTIC LASER SCANNER

ISOMET

March 1987

The LS110-XY provides high speed simultaneous vertical and horizontal axis beam position control at visible and near IR wavelengths. It is comprised of two orthogonally-mounted single-axis TeO_2 deflectors which sequentially diffract the input laser beam to generate up to a 750 x 750 spot combined matrix. The LS110-XY may be operated in raster (linear), random access and vector scanning modes from the same RF drive electronics. It is well suited for applications requiring accurate beam placement at high speed, such as laser rangefinding and laser pantography.

SPECIFICATIONS

	MODELS		
	LS110-633XY	LS110-830XY	LS110-1.06XY
Wavelength:	633nm	830nm	1.06µm
Center Frequency:	100MHz	50MHz	50MHz
Bandwidth, Δf:	50MHz	25MHz	25MHz
Scan Angle/Axis:	2.9°	1.9°	2.5°
f_c Separation Angle/ Axis:	5.9°	3.9°	4.9°
Resolution (τΔf):	750x750	375x375	375x375

ALL MODELS

Access Time, τ:	15µsec (maximum)
Input Aperture:	9.3mm diameter
Input Laser Polarization:	Linear
Output Laser Polarization:	Circular (nominal)
Thruput Efficiency:	> 25%
Input Impedance:	50Ω (nominal)
RF Drive Electronics:	(2 each) Model D100A-2 OR (2 each) Models VCO-200A, IA-100, RFA-1108.

Crystal Technology, Inc.

Acousto-Optic Deflectors and Bragg Cells

Wide Bandwidth Bragg Cells

SPECIFICATIONS

Values are for operation at 633 nm. Diffraction efficiency at 830 nm will be approximately 40% of the 633 value.

Model Number	Mode	Wavelength (nm)	Center Frequency (GHz)	3 dB Bandwidth (GHz)	Time Aperture (μsec)	Time Bandwidth Product	Aperture Dimensions (mm)
41000L-LN	Long	633–830	1	0.5	2	1000	0.2 × 18
41000L-GP	Long	633–830	1	0.5	0.3	150	0.1 × 2
41000L-GP-PA Phased Array	Long	830	1	0.5	0.3	150	0.07 × 2
41000S-GP	Shear	830	1	0.5	1	500	0.05 × 5
41500S-GP	Shear	830	1.5	1	0.5	500	0.05 × 2.1
42000L-GP	Long	830	2	1	0.1	100	0.05 × 0.7
42000L-LN	Long	633–830	2	1	1	1000	0.05 × 7
42000S-LN	Shear	830	2	1	0.3	300	0.05 × 1

*Measured with a fully illuminated beam over the entire active aperture.

FEATURES

- Instantaneous bandwidths of 1000 MHz
- Scan times as low as 150 nanoseconds
- Ability to sort simultaneous in-band signals
- Capability for 100% probability of intercept
- Polarization switching for increased dynamic range (Model 42300S-LN)

The highest quality Lithium Niobate ($LiNbO_3$) and Gallium Phosphide (GaP) materials are used to make ultra-wide bandwidth Bragg cells for operation between 633 and 830 nm.

OPERATING CHARACTERISTICS

Wavelengths . . . . . 633 to 850 nm
Static Contrast Ratio . . . . . 40 dB min
Optical Wavefront Distortion . . . . . λ/6 typ
λ/4 max
VSWR . . . . . 2:1 max over 0.5 GHz
2.5:1 max over 1.0 GHz

Model numbers indicate the following:

4 2 X – XX

- XX — Optical Material (LN = $LiNbO_3$, GP = GaP)
- X — Acoustic Mode (L = Longitudinal, S = Shear)
- 2 — Typical Center Frequency (in GHz)
- 4 — Beam Deflector Series

Crystal Technology, Inc.

Acousto-Optic Deflectors and Bragg Cells

Wide Bandwidth Bragg Cells

SPECIFICATIONS

Model Number	Max RF Drive Power (Watts)	Polarization	Optical Transmission	Acoustic Velocity (mm/μsec)	Acoustic Attenuation (dB/μsec/GHz^2)	Remarks
41000L-LN	1.5	Vertical	96	6.57	1.0	High Resolution
41000L-GP	1.0	Horizontal	80	6.46	8	High Efficiency
41000L-GP-PA Phased Array	1.0	Horizontal	80	6.4	8	Phased Array Transducer for Max Efficiency
41000S-GP	0.7	H or V	80	4.13	2.1	Polarization Switching/High Resolution
41500S-GP	0.7	H or V	80	4.13	2.1	High Resolution
42000L-GP	0.7	Horizontal	80	6.46	8	High Efficiency
42000L-LN	1.0	Vertical	96	6.57	1.0	High Resolution
42000S-LN	1.0	Vertical	96	3.44	1.5	Polarization Switching

Polarization — Vertical is perpendicular to acoustic propagation.

Crystal Technology, Inc.

Acousto-Optic Deflectors and Bragg Cells

Large Aperture, High Resolution Bragg Cells

PERFORMANCE SUMMARY

Optical Material	Tellurium dioxide (TeO_2)
Acoustic Mode	Slow shear (110)
Optical Propagation	(001)
Optical Polarization	Elliptical (slow mode input)
Input Impedance	50 ohms
VSWR (over bandwidth)	< 3:1, goal of 2:1
Maximum Drive Power	1.5 watts
Anti-reflection coating	< 1%/surface
Surface Finish	20-10
Wavefront Distortion	< λ/6 (transmitted)
Crystal Orientation	< 2 arc min
Parallelism	< 2.5 arc min
Connector	SMA female

Model	Center Frequency (MHz)	Bandwidth (MHz)	Wavelength (nm)	Aperture Time (μsec)	Clear Aperture (mm)	Diffraction Efficiency* (%/watt)
4050-1A	50	30	633	40	12 × 30	225
4050-1B	50	30	830	40	12 × 30	75
4050-2A	50	30	633	70	12 × 43.5	135
4050-2B	50	30	830	70	12 × 43.5	45
4050-3A	50	30	633	80	12 × 53	120
4050-3B	50	30	830	80	12 × 53	35
4075-1A	75	50	633	40	12 × 30	80
4075-1B	75	50	830	40	12 × 30	25
4075-2A	75	50	633	70	12 × 43.5	40
4075-2B	75	50	830	70	12 × 43.5	17.5
4075-3A	75	50	633	80	12 × 53	30
4075-3B	75	50	830	80	12 × 53	15

Crystal Technology, Inc.

Acousto-Optic Scanner

Model 4080

PERFORMANCE SUMMARY

Optical Material	TeO_2
Mode	Slow shear, off-axis
Center Frequency	80 MHz
Bandwidth	50 MHz
Diffraction Efficiency	80% nominal
Output Flatness	±10% maximum at full rated output
Input Polarization	Linear, parallel to base plate
Output Polarization	Linear, vertical to base plate
RF Drive Power	<1 watt for Models -1 and -2 <2 watts for Models -3 and -4

Model	Wavelength* (nm)	Access Time (μsec)	Resolvable Spots	Active Aperture (mm)
4080-1	488–633	10	500	2×8
4080-2	488–633	20	1000	2×14
4080-3	830–1.060	10	500	2×8
4080-4	830–1.060	20	1000	2×14

*Other wavelengths available upon request.

APPENDIX C. FEED COMPUTER CODE

The Fortran code which was designed to analyze the OFEED system is presented. Comments are spaced throughout the program for clarity.

```
C FORTRAN PROGRAM:  FEED
C
C  This program calculates the optical interference scan angle
C  (DTHETA), the fiber positions (FP) and the antenna element
C  positions (Z) along the Z-axis.  It also calculates what the
C  antenna scan angle (SCAN) will be.  It creates an output file
C  suitable for input to the ARRPAT program.
C
C  It prompts for inputs: AO bandwidth being scanned (DFREQ),
C  AO velocity (V), optical wavelength (LAMBDA), fiber spacing
C  (S), number of elements (N), and type of elements (TYPE).
C
      INTEGER N,I,J
      REAL DFREQ,V,LAMBDA,DTHETA,OIA,SCAN,S,HZ,HS,X,X2,DEN,D
      DIMENSION ALPHA(20), Z(20), FP(20)
      PI=3.14159265
      RTD=180./PI
C
C  User inputs
      WRITE(1,100) " AO BANDWIDTH IN MHZ = "
100   FORMAT(/,' ',A0 $)
      READ(1,200) DFREQ
200   FORMAT(G0.0)
      WRITE(1,100) " AO VELOCITY IN M/S = "
      READ(1,200) V
      WRITE(1,100) " OPTICAL WAVELENGTH IN NANOMETERS = "
      READ(1,200) LAMBDA
      WRITE(1,100) " FIBER SPACING IN MICROMETERS = "
      READ(1,200) S
      WRITE(1,100) " NUMBER OF ELEMENTS IN ARRAY = "
      READ(1,300) N
300   FORMAT(I2)
      WRITE(1,100) " ISOTROPIC (0) or HALF-WAVE DIPOLES (2) ? "
      READ(1,300) TYPE
C
      IF (IOWRIT(6,2,0,"INPUT")) GOTO 99
      WRITE(6,35) N,TYPE,0
35    FORMAT(' ',3I2)
      DFREQ=DFREQ*1.0E06
      LAMBDA=LAMBDA*1.0E-09
      S=S*1.0E-06
C
C  Interference angle calculation
      DTHETA=2.0*DFREQ*LAMBDA/V
      OIA=DTHETA*RTD
      WRITE(1,400) "OPTICAL INTERFERENCE ANGLE (DEG) = "
400   FORMAT(///,' ',A0 $)
      WRITE(1,45) OIA
      WRITE(1,55) " ANTENNA ELEMENT SPACINGS ARE ASSUMED TO BE
     1  HALF WAVELENGTH."
```

```
C  Calculate positions
        D=N/2.0
        I=INT(N/2.0)
        E=FLOAT(I)
        IF(D.GT.E) GOTO 15
        HZ=0.25
        HS=S/2.0
        Z(I)=-HZ
        FP(I)=-HS
25      J=I+1
        DO 10 I=J,N
        Z(I)=Z(I-1)+0.5
        FP(I)=FP(I-1)+S
10      CONTINUE
        J=J-2
20      I=J
        Z(I)=Z(I+1)-0.5
        FP(I)=FP(I+1)-S
        J=J-1
        IF(J.GT.0) GOTO 20
        WRITE(1,55) " CALCULATED GEOMETRY AND PHASES "
55      FORMAT(/, ' ',A0,/)
C
C  Calculate phases
        DO 30 I=1,N
        ALPHA(I)=2.0*PI*FP(I)*DTHETA/LAMBDA
        ALPHA(I)=ALPHA(I)*RTD
        WRITE(1,45) 0.0,0.0,Z(I),1.0,ALPHA(I)
        WRITE(6,45) 0.0,0.0,Z(I),1.0,ALPHA(I)
45      FORMAT(6F10.4)
30      CONTINUE
C
C  Calculate antenna scan angle
        X=4.0*S*DFREQ/V
        X2=X*X
        DEN=SQRT(1.0-X2)
        SCAN=ATAN(X/DEN)
        SCAN=SCAN*RTD
        WRITE(1,65)
65      FORMAT(/)
        WRITE(1) " MAXIMUM ANTENNA SCAN ANGLE (DEGREES) = "
        WRITE(1,45) SCAN
        WRITE(1,55) " THIS ANGLE IS WITH RESPECT TO ARRAY NORMAL.
     1    ARRPAT computes the angle with respect to
     1   the array endfire.  Thus the ARRPAT scan
     1 angle will be: 90 degrees plus this scan angle."
        GOTO 98
C
15      I=I+1
        Z(I)=0.0
        FP(I)=0.0
        GOTO 25
98      IF(IOCLOS(6)) GOTO 99
99      STOP
        END
```

REFERENCES

1. A. Daryoush, P. Herczfeld, V. Contarino, A. Rosen, Z. Turski, and P. Wahi, "Optical Beam Control of MM-Wave Phased Array Antennas for Communications," Microwave Journal, March 1987, p. 97.

2. P. R. Herczfeld, A. S. Daryoush, M. Kieli, S. Siegel, and R. Soref, "Wide-Band True Time Delay Phase Shifter Devices," IEEE MTT-S Digest, 1987, p. 603.

3. Richard A. Soref, U.S. Patent No. 4,671,604, June '87.

4. P. G. Sheehan and J. R. Forrest, "The Use of Optical Techniques for Beamforming in Phased Arrays," Optical Technology for Microwave Applications, SPIE Vol. 477, 1984, p. 82.

5. Ted Leonard, telephone conversation Aug. 1988, Alcatel, Roanoke, VA.

6. R. J. Mailloux, "Phased Array Theory and Technology," Proceedings IEEE, Vol. 70, Mar. 1982, p. 246.

7. A. Rosen, P. Stabile, P. Herczfeld, A. Daryoush, and V. Contarino, "Optically Controlled Microwave Devices and Circuits," RCA Review, Vol. 46, Dec. 1985, p.528.

8. A. Rosen, P. Stabile, and P. Herczfeld, "Optically Controlled Lateral PIN Diodes and Microwave Control Circuits," RCA Review, Vol. 47, Dec. 1986, p. 443.

9. N. Jespersen, P. Herczfeld, A. Rosen, and P. Stabile, "Optically Controlled Beamforming For Phased Array Antennas," IEEE 1986 International Symposium Antennas & Propagation, Vol. 1, June 1986, p. 357.

10. L. Brothers, Jr. and C. Cox, III, "A High-Speed Phase Shifter Based on Optical Injection," IEEE MTT-S Digest, 1987, p. 819.

11. Richard A. Soref, "Voltage-Controlled Optical/RF Phase Shifter," Journal of Lightwave Technology, Vol. LT-3, No. 5, Oct. 1985, p. 992.

12. Gerhard A. Koepf, "Optical Processor For Phased-Array Antenna Beam Formation," Optical Technology for Microwave Applications, SPIE Vol. 477, 1984, p. 75.

13. M. Tamburrini, M. Parent, L. Goldberg, D. Stillwell, "Optical Feed For A Phased Array Microwave Antenna," Electronics Letters, Vol. 23, No. 13, June 1987, p. 680.

14. Paul A. Tipler, Physics, Worth Publishers, Inc., New York, 1978.

15. Allen Nussbaum and Richard A. Phillips, Contemporary Optics for Scientists and Engineers, Prentice-Hall, Inc., New Jersey, 1976.

16. Eddie H. Young, Jr. and Shi-Kay Yao, "Design Considerations for Acousto-Optic Devices," Proceedings of the IEEE, Vol. 49, No. 1, January 1981, p. 54.

17. Stewart E. Miller and Alan G. Chynoweth, Editors, Optical Fiber Telecommunications, Academic Press, New York, 1979.

18. Practical Phased-Array Systems, Microwave Journal Intensive Course, Horizon House, San Francisco, April 1975.

19. Michael K. Barnoski, Editor, Fundamentals of Optical Fiber Communications, Academic Press, New York, 1981.

20. Shi-Kay Yao, "Wideband Bragg Cell Efficiency Enhancement Techniques," Optical Technology for Microwave Applications II, SPIE Vol. 545, 1985, p. 72.

21. Warren L. Stutzman and Gary A. Thiele, Antenna Theory and Design, John Wiley & Sons, Inc., New York, 1981.

22. Dale Ehrhart, telephone conversation Aug. 1988, Brimrose Technology, Baltimore, MD.

23. T. R. Joseph, W. E. Stephens, and B. U. Chen, "Fiber Optic RF Links," Optical Technology for Microwave Applications, SPIE Vol. 477, 1984, p.52.

24. F. Safet-Peyman and I. C. Chang, "Diffraction and Detection of Bulk Acoustic Waves," Optical Technology for Microwave Applications II, SPIE Vol 545, 1985, p.58.

25. Irwin J. Abramovitz, "Passive Surveillance Applications of Acousto-Optic Processors," Optical Technology for Microwave Applications II, SPIE Vol 545, 1985, p.102.

26. C. M. Gee and G. D. Thurmond, "Wideband Traveling-Wave Electro-Optic Modulator," Optical Technology for Microwave Applications, SPIE Vol 477, 1984, p. 17.

27. V. M. Contarino, A. S. Daryoush, and P. R. Herczfeld, "Large-Signal Modulation of Semiconductor Lasers With Optical Feedback for Millimeter Wave Applications," IEEE MTT-S Digest, 1987, p. 653.

28. A. S. Daryoush, P. R. Herczfeld, A. Rosen, A. Sharma, and V. Contarino, "Subharmonic Indirect Optical Injection Locking of a Millimeter Wave IMPATT Oscillator," Proceedings IEEE MTT-S International Microwave Symposium, 1986, p. 109.

29. Irwin J. Abramovitz and A. P. Goutzoulis, "Digital Electronics Meets Its Match," IEEE Spectrum, August 1988, p. 21.

The vita has been removed from the scanned document